Geophysical characterisation of the groundwater-surface water interface

P. J. McLachlan[1,*], J.E. Chambers[2], S. S. Uhlemann[2, 3], A. Binley[1]

1 – Lancaster Environment Centre, Lancaster University, Lancaster, UK

2 – Geophysical Tomography Team, British Geological Survey, Nottingham, UK

3 – ETH Zurich, Institute of Geophysics, Zurich, Switzerland

[*] Corresponding author: P. J. McLachlan, p.mclachlan@lancaster.ac.uk

Abstract

Interactions between groundwater (GW) and surface water (SW) have important implications for water quantity, water quality, and ecological health. The subsurface region proximal to SW bodies, the GW-SW interface, is crucial as it actively regulates the transfer of nutrients, contaminants, and water between GW systems and SW environments. However, geological, hydrological, and biogeochemical heterogeneity in the GW-SW interface makes it difficult to characterise with direct observations. Over the past two decades geophysics has been increasingly used to characterise spatial and temporal variability throughout the GW-SW interface. Geophysics is a powerful tool in evaluating structural heterogeneity, revealing zones of GW discharge, and monitoring hydrological processes. Geophysics should be used alongside traditional hydrological and biogeochemical methods to provide additional information about the subsurface. Further integration of commonly used geophysical techniques, and adoption of emerging techniques, has the potential to improve understanding of the properties and processes of the GW-SW interface, and ultimately the implications for water quality and environmental health.

Key words

Groundwater-surface water interactions, Hyporheic zone, Hydrogeophysics, Geophysics

1. Introduction

It is widely recognised that groundwater (GW) and surface water (SW) form a continuum and are not isolated components (Winter et al., 1998; Malard et al., 2002; Sophocleous, 2002). GW-SW interactions have significant implications for water quantity, water quality, and health of aquatic ecosystems, at site to catchment scales (Winter et al., 1976; Stanford and Ward, 1993; Findlay, 1995; Boulton et al., 1998; 2010; Buss et al., 2009; Harvey and Gooseff, 2015). For instance, contaminated GW discharge can degrade streams, lakes, deltas and wetlands, and associated habitats; conversely GW discharge may also supply vital nutrients and act as a thermal buffer to maintain ecological function (Power et al. 1999; Hayashi and Rosenberry 2002; Marzadri et al., 2013a, b). Over-abstraction of GW can also result in the redistribution or disappearance of SW resources (Winter et al., 1998), and in coastal regions, the contamination of fresh water aquifers (Ingham et al., 2006).

The transition zone between SW environments and GW systems, the GW-SW interface, is important as it governs the exchange of water, nutrients, and pollutants (Buss et al., 2009; Kalbus et al., 2006; Fleckenstein et al., 2010; Lin et al., 2010; Lansdown et al., 2015). Despite conceptually representing an interface, the term GW-SW interface is commonly used to describe alluvial sediments proximal to SW bodies, e.g. stream beds, lake beds, riparian zones, and flood plains. Therefore, it typically has vertical extents up to several metres and horizontal extents on the order of hundreds of metres. It is important to note here that the term GW-SW interface is not synonymous with the hyporheic zone (HZ). Particular interest has been given to the HZ because of its role in biogeochemical cycling; however its definition is ambiguous and discipline dependent (Stanford and Ward, 1988; Triska et al., 1989; Tonina and Buffington, 2009; Boulton et al., 2010; Ward, 2016; Hester et al., 2017). It is perhaps best described as the region of the GW-SW interface that occurs non-continuously in both

space and time, and permits the residence of both GW and SW (e.g. Gooseff, 2010). The HZ is therefore not ubiquitous, as is commonly assumed and is often limited to narrow zones (Hester et al., 2013; 2017). The physical dimensions of the hyporheic zone are also difficult to define, however, the majority of HZ studies focus on lateral scales of 1-10 m and vertical scales of <1 m (Ward, 2016). Although traditionally used to refer to mixed regions in the vertical vicinity of rivers, there has been the tendency to group the HZ with GW-SW mixing in lateral to SW bodies, e.g. the riparian zone, with regions being referred to as fluvial HZs zones and floodplain HZs (Mitsch, 1992; Gilliam, 1994; Edwards, 1998; Tonina and Buffington, 2009; Boano et al., 2014)

There are numerous established methods that exist for characterisation of the GW-SW interface (Cook and Herczeg, 2000; Stonestrom and Constantz, 2003; Bridge et al., 2005; Greswell et al., 2005; Kalbus et al., 2006; Rosenberry and LaBaugh, 2008; Fleckenstein et al., 2010). However, despite providing direct measurements, use of piezometers, seepagemeters, and boreholes may be limited by site conditions, environmental protection, or installation costs. In this way information may be spatially limited and not representative. Conversely, tracer experiments (e.g. Findlay et al., 1993; Triska et al., 1993; Harvey et al., 1996; Harvey and Fuller, 1998; González-Pinzón et al., 2015; Xie et al., 2016) provide information that is averaged over larger volumes and therefore may fail to characterise spatial heterogeneity, e.g. identifying low mobility and high mobility zones in the subsurface (Singha et al., 2008).

In the past two decades, near surface geophysics has been increasingly used in characterisation of the GW-SW interface, in addition to other environmental applications (Binley et al., 2015; Parsekian et al., 2015; Singha et al., 2015). Geophysical techniques are sensitive to geophysical properties of the subsurface and hence act as proxies for geological, hydrological, and biogeochemical parameters. It is important to note that while advances in geophysical instruments and subsequent modelling have allowed for more reliable data interpretation, geophysical data can still be ambiguous and often special consideration is required for the deployment of geophysical tools in

different settings. Nonetheless, geophysical tools offer the unprecedented opportunity to characterise subsurface parameters at vertical scales of centimetres to hundreds of metres, horizontal scales of metres to hundreds of metres, and temporal resolutions of minutes to hours. Furthermore, given that multidisciplinary research has been essential in GW-SW interface research (Newbold, 1982; Bencala, 1984; Valett et al., 1993**;** Sophocleous, 2002; Wojnar et al., 2013; Ward, 2016), the wider application of geophysical tools would be beneficial. However, it is essential that geophysics is used to address hydrogeological or biochemical problems, rather than hydrogeological or biogeochemical solutions being used to explain geophysical results.

This review focuses on various geophysical tools relevant to characterising properties and processes of the GW-SW interface. In this review, the GW-SW interface and GW-SW interactions are first considered, common geophysical approaches are outlined, various geophysical applications are then reviewed, and finally, avenues of future research are discussed. Although important in governing zones of GW-SW interaction, more general geophysical studies investigating properties of the bedrock aquifers are not included here, but have been the subject of a number of reviews (e.g. Rubin and Hubbard, 2005; Linde et al., 2006; Singha et al., 2007; Holliger, 2008; Hubbard and Linde, 2011; Binley et al., 2015; Singha et al., 2015; Boago, 2017). However, large scale airborne geophysical studies, which typically sense to depths of tens to hundreds of metres, are considered as they have the potential to provide a large scale context for processes occurring across the GW-SW interface. These applications fit well into the requirements of GW-SW interactions to be considered at catchment scales (Kaika, 2003; Buss et al., 2009; Harvey and Gooseff, 2015).

2. The Groundwater-surface water interface

The GW-SW interface is subjected to exchanges spanning multiple spatial scales (Tóth, 1963; Woessner, 2000). At large scales, GW flow paths are principally influenced by hydrostatic forces arising from topography and geology, and occur on scales of metres to hundreds of kilometres (Tóth, 1963; Freeze and Witherspoon, 1967; Winter et al., 1998). On smaller scales, flow paths originating

in the SW may temporarily enter the subsurface and allow for GW-SW mixing. These flow paths are commonly referred to as hyporheic exchange flows (HEFs) and are principally governed by geomorphological features (Elliot and Brooks, 1997; Käser et al., 2009; Boano et al., 2014; Hester et al., 2017). HEFs are generally reported to be driven by hydrodynamic forces induced by sand dunes, and cobbles at millimetre to centimetre scales or by hydrostatic forces generated by pool-riffle sequences, sediment bars, meanders, and riparian zones at metres to tens of metres (Harvey et al., 1996; Woessner, 2000; Lautz and Siegel, 2006; Tonina and Buffington, 2007; 2009; Käser et al., 2009; 2013; Stonedahl et al., 2010; 2013; Boano et al., 2014). In this way, hydrological pathways are typically viewed as being nested within in each other (Figure 1). In reality, this distinction is somewhat arbitrary as HEFs have been stated to occur laterally over hundreds of metres (Boano et al., 2014). Ideally, the point at which the water originating from SW more closely resembles the GW is the point at which it becomes groundwater recharge regardless of where and when it returns to the surface.

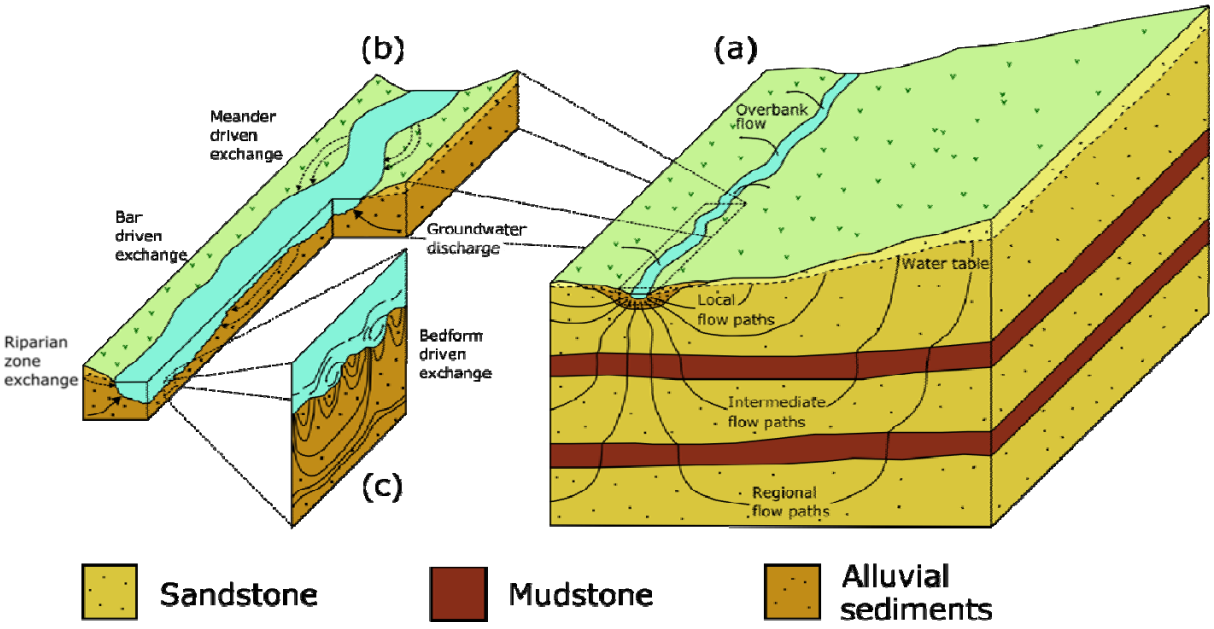

112 Figure 1: (a) Various scales of groundwater flow paths and their relation to (b) macro-scale and (c)
113 micro-scale exchanges in a fluvial and floodplain hyporheic zones (after Tóth, 1963; Winter et al.,
114 1998; Stonedahl et al., 2010).

115 The GW-SW interface is also influenced by temporal variability across scales of milliseconds to years.
116 For instance, turbulent flow in rivers can drive GW-SW mixing within several millimetres of the
117 sediment-water interface on timescales of milliseconds to seconds (Menichino and Hester, 2014;
118 Chandler et al., 2016). On larger timescales, periodic variations in precipitation, snowmelt,
119 evapotranspiration, and flood pulses can modify, or reverse, GW-SW interactions (Boano et al.,
120 2008; Loheide and Lundquist, 2009; Wondzell et al., 2010; Larsen et al., 2014; Zimmer and Lautz;
121 2014; Dudley-Southern and Binley, 2015; Malzone et al., 2016; Schmadel et al., 2016). GW-SW
122 interactions can also be influenced by waves and tides (Harvey et al., 1987; King et al., 2009;
123 Bianchin et al., 2011), or driven by density contrasts (Musgrave and Reeburgh, 1982; Webster et al.,
124 1996; Boano et al., 2009).

125 Properties and processes of the GW-SW interface are therefore highly spatially and temporally
126 heterogeneous. Heterogeneity in alluvial deposits can influence permeability, dispersivity,
127 subsurface residence times, and zones of GW-SW exchange. Also bedrock aquifers can dictate
128 whether interaction are localised (e.g. in fractured or karstic settings) or distributed (e.g. in clastic
129 aquifers), and consequently they influence hydrological and biogeochemical conditions at the GW-
130 SW interface (Nagorski and Moore, 1999; Gandy et al., 2007; Kennedy et al., 2009). Temporal
131 variability in hydrostatic forces can influence locations and timings of GW-SW interactions, the
132 interaction of GW discharge and HEFs, and consequently biogeochemical reactions (Boano et al.,
133 2014). Biogeochemical properties, such as cation exchange capacity, redox gradients, and thermal
134 gradients, have long been known to be important (Bencala et al., 1984; von Gunten et al., 1991;
135 Winter et al., 1998; Power et al., 1999) but are highly variable, making it difficult to predict pollutant
136 attenuation and nutrient cycling. Furthermore, there have been a limited number of investigations

into HZ and GW-SW interface processes across different orders of streams and their relevance to the catchment (e.g. Gomez-Velez and Harvey, 2014; Kiel and Cardenas, 2014; Marzadri et al., 2017). Therefore, field methods that provide spatially and temporally complete data sets about geological, hydrological, and biogeochemical information at site to catchment scales are required (Buss et al., 2009; Boano et al., 2014; Harvey and Gooseff, 2015; Ward et al., 2016; Hester et al., 2017).

3. Geophysical approaches

The general premise of geophysics is to obtain information about the geophysical properties of the subsurface to infer information about geological, hydrological, and biogeochemical properties (Binley et al., 2015). Geophysical properties can be interpreted using petrophysical models, calibration with other methodologies (both non-geophysical and geophysical), and analysis of temporal data sets of dynamic processes. Geophysical techniques considered here are electrical resistivity (ER), induced polarisation (IP), self-potential (SP), electromagnetic induction (EMI), ground penetrating radar (GPR), and seismic methods (Table 1). Furthermore, forward, inverse, and petrophysical modelling are also briefly discussed due to their importance in data interpretation. Fundamental geophysical theory (e.g. Telford et al., 2010) is beyond the scope of this section, and instead focus is given to the basic principles of field and modelling techniques. Applications of temperature sensing in GW-SW interface studies are also beyond the scope of this review (Stonestrom and Constantz, 2003; Irvine and Lautz, 2015; Hare et al., 2015; Irvine et al., 2016; Wilson et al., 2016).

Table 1 – Geophysical techniques and the parameters which they relate to. Rough indications of investigation depths and temporal resolution are also included. In practice, terrestrial surveys typically involve horizontal scales of metres to hundreds of metres, whereas for waterborne and airborne surveys, horizontal extents may be metres to tens of kilometres and hundreds of metres to hundreds of kilometres, respectively.

Geophysical Technique	Geophysical Properties	Examples of Derived Environmental Parameters	Typical Investigation Depths	Typical Acquisition Time for 100 m Transect
Electrical Resistivity	Electrical Conductivity	Water Content, Clay Content, Pore Water Conductivity, Porosity, Stratigraphy	Metres to Tens of Metres	Tens of Minutes
Induced Polarisation	Electrical Conductivity, Chargeability	Water Content, Clay Content, Pore Water Conductivity, Surface Area, Permeability, Stratigraphy	Metres to Tens of Metres	Tens of Minutes to Hours
Spectral Induced Polarisation	Electrical Conductivity, Chargeability (with Frequency Dependency)	Water Content, Clay Content, Pore Water Conductivity, Surface Area, Permeability, Stratigraphy	Metres to Tens of Metres	Tens of Minutes to Hours
Self-Potential	Electrical Potential	Hydrological Flux, Permeability, Redox Gradients	Metres	Seconds to Minutes
Electromagnetic Induction	Electrical Conductivity	Water Content, Clay Content, Salinity	Metres to Hundreds of Metres	Seconds to Minutes
Ground Penetrating Radar	Dielectric Permittivity, Electrical Conductivity	Water Content, Porosity, Stratigraphy	Metres to Tens of Metres	Minutes to Tens of Minutes
Seismic	Bulk Density, Elastic Moduli	Porosity, Stratigraphy	Metres to Tens of Metres	Tens of Minutes

3.1. Electrical resistivity

ER methods are used to determine subsurface electrical resistivity by injecting low frequency (<1 kHz) electrical currents into the ground with two current electrodes and measuring the resultant voltage between two or more potential electrodes (Binley, 2015). ER methods are typically minimally invasive as they commonly involve placing stainless steel electrodes several centimetres into the subsurface, however, in some cases borehole ER is used for enhanced characterisation (e.g. Slater et al., 1997; Crook et al., 2008; Wilkinson et al., 2010; Coscia et al., 2011; 2012). In environmental applications the ER signal is typically dependent on the characteristics of the pore fluid and grain-fluid interface (Glover, 2015). Modern ER instruments are capable of systematically using different combinations of electrodes arranged in lines or grids to image the subsurface in 2D or 3D surveys (Loke et al., 2013). These types of surveys are often referred to as ER imaging (ERI) or ER tomography (ERT). In addition to 2D and 3D surveys, temporally distributed measurements can be used to monitor dynamic processes (e.g. Ward et al., 2010a; Johnson et al., 2012; Uhlemann et al., 2016).

3.2. Induced polarisation

IP methods are effectively an extension of ER methods and use low frequency (<1 kHz) currents to assess the capacitive properties of the subsurface (Binley, 2015). The IP signal typically arises due to

179 the temporary accumulation of ions in porous media following the injection of an electric current
180 (Kemna et al., 2012). Whereas the ER signal is dependent on the properties of both the pore fluid
181 and the porous media, the IP signal is more closely associated with the properties of the grain-fluid
182 interface (Revil et al., 2012). IP can therefore provide information about lithological properties with
183 minimal interference from pore water conductivity (Vinegar and Waxman, 1984; Kemna et al., 2000;
184 Lesmes and Frye 2001; Weller et al., 2013; Glover, 2015). As with ER methods, IP measurements can
185 be made using two current electrodes and two potential electrodes. Modern multichannel systems
186 permit the use of multiple potential dipoles simultaneously in an array to record the full-waveform
187 of the IP signal. Induced polarisation can be conducted in either the time or the frequency domain
188 (Revil et al., 2012). Time domain IP methods involve injecting a direct electrical current between the
189 current electrodes before abruptly switching it off and measuring the voltage decay over a specific
190 time interval between the potential electrodes. Frequency domain IP involves injecting alternating
191 electrical currents and measuring the impedance and the phase lag of the current and voltage
192 waves. Frequency domain IP methods can also be carried out using multiple frequencies to assess
193 the frequency dependent impedance and phase shift between injected current and measured
194 voltage, this is typically referred to as spectral IP (SIP).

195 ### 3.3. Self-potential

196 Unlike ER and IP methods, SP methods are passive in that they measure naturally occurring voltages
197 within the subsurface (Jackson, 2015). The SP method is relatively simple in that voltages can be
198 measured using non-polarising electrodes and a high impedance voltmeter (Minsley et al., 2007).
199 Non-polarising electrodes are required to minimise polarisation at the electrode interface and a high
200 impedance voltmeter is required to avoid drawing current from the ground. Under natural
201 conditions the SP signals arise from electro-kinetic, electro-chemical and thermo-electric effects
202 (Wynn and Sherwood, 1986; Revil et al., 2012; Jackson, 2015). The electro-kinetic effect, or
203 streaming potential, arises from the advective transfer of excess charges through porous materials

(Rizzo et al., 2004). The electro-chemical effect originates from the presence of ion and electron concentration gradients, such as those resulting from redox conditions (Sato and Mooney, 1960; Revil et al., 2010). The thermo-electric effect is caused by the differential thermal diffusion of ions in the pore fluid and donor electrodes in porous media (Wynn and Sherwood, 1986).

3.4. Electromagnetic induction

Whereas ER, IP, and SP use low frequency (<1 kHz) electrical currents, electromagnetic methods (e.g. EMI and GPR) use higher frequency signals to induce electromagnetic effects in the subsurface. EMI instruments operate in either the frequency domain (FD-EMI) or the time domain (TD-EMI) and use primary and secondary coils to determine subsurface electrical conductivity and magnetic susceptibility (Everett and Meju, 2005; Fitterman, 2015). In FD-EMI systems a primary current with a specific angular frequency is generated in the primary coil; this induces a primary magnetic field that is out-of-phase with the initial current. The primary magnetic field creates an electromagnetic force that induces eddy currents in the subsurface and a consequent secondary magnetic field. The secondary magnetic field is detected by the secondary coil and is used to infer information about in-phase and out-of-phase components of the subsurface electrical properties. In TD-EMI systems, a current is typically passed around the primary coil before it is abruptly switched off. This current generates a primary magnetic field which induces an electromagnetic force, both of which are in-phase with the primary current. The electromagnetic force generates eddy currents that decay by ohmic dissipation following termination of the primary current. The decay of the eddy currents produces a secondary magnetic field and its rate of change through time is measured by the secondary coil to infer subsurface conductivity (Nabighian and Macnae, 1991). Modern FD-EMI instruments contain multiple secondary coils and can be used to detect information from several depths simultaneously. EMI systems have advantages over electrical methods in that they do not require contact with the subsurface, allowing for easier usage in waterborne or airborne surveys (e.g. Butler et al., 2004; Binley et al., 2013; Harrington et al., 2014).

3.5. Ground penetrating radar

As with EMI, GPR methods use electromagnetic signals to assess subsurface properties. However the frequencies used in GPR are higher (10 MHz to 2 GHz), such that the signal travels by wave propagation, rather than by diffusion. In GPR systems a high frequency signal is emitted into the subsurface via a transmitter antenna before it travels to the receiver antenna, e.g. by reflection from an interface of contrasting electrical properties (Annan , 2005; Huisman et al., 2013; van der Kruk, 2015). The amplitudes and travel times of the returning waves are then used to determine dielectric properties and locate boundaries in the subsurface. Field studies often involve time domain GPR systems and typically use frequencies between 50 and 500 MHz. Frequency domain systems are also available, and in some cases using wider bandwidth permits more accurate modelling of the subsurface (Lambot et al., 2004; 2006). The depth of penetration of the signal is dependent upon the electrical conductivity of the subsurface and the frequencies used. Due to frequency dependent attenuation mechanisms, higher frequencies do not penetrate to as great depths but generally permit higher resolution images. Furthermore, highly electrically conductive environments may attenuate the signal and reduce the penetration depth.

3.6. Seismic methods

Seismic methods operate in a similar fashion to GPR but use the propagation of acoustic energy to infer information about the mechanical properties of the subsurface (Steeples, 2005; Schmitt, 2015). Seismic surveys can be conducted by generating waves with an acoustic source (e.g. a sledgehammer). When these waves reach boundaries of contrasting mechanical properties, some energy reflects off the boundary and some energy refracts along the boundary. Returning seismic waves are detected by a series of receivers (geophones) on the surface and can be used to calculate seismic wave velocity, mechanical impedance, elastic moduli, and determine the locations of structural boundaries.

3.7. Geophysical modelling

Forward modelling is used to calculate the data that would theoretically be observed for a given distribution of geophysical properties. The underlying principles of geophysical methods are well understood, so the creation of synthetic data sets from a model of geophysical properties is straight forward (Binley, 2015). Forward modelling serves two key purposes: (1) to aid survey design and (2) to assist in inversion and interpretation of data. For instance, different geophysical methods and measurement schemes have different strengths and weaknesses. Therefore, by making reasonable estimates of the subsurface properties, the usefulness of a geophysical technique can be assessed prior to its deployment (Terry et al., 2017). Forward modelling may also be useful in guiding interpretation of unusual features, and prior to sufficient computational power, geophysical data was often interpreted by comparing data with forward models, such as ER sounding curves (Loke et al., 2013).

Inverse modelling is the process of determining the distribution of subsurface geophysical properties based on observed geophysical data and any prior information. The principles of geophysical inversion are beyond the scope of this paper but information can be found elsewhere (e.g. Aster et al., 2005; Tarantola, 2005; Menke, 2012; Linde et al., 2015). The majority of inverse problems are non-unique in that there can be an infinite number of solutions for one geophysical data set. In order to constrain the inversions, regularisation may be used to introduce assumptions to prevent over fitting of data and encourage unique solutions, e.g. lateral smoothing in stratified deposits (Constable et al., 1987; Tarantola, 2005). Moreover, uncertainty can further be reduced by carrying out joint or coupled inversions. In hydrogeophysics, joint inversions involve incorporation of various geophysical and hydrogeological data sets (e.g. Linde et al., 2006; Herckenrath et al., 2013) while coupled inversions model geophysical data within the bounds of prior hydrological models (e.g. Hinnell et al., 2010; Huisman et al., 2010).

277 In order to be of use in hydrogeology, geophysical models are often interpreted in terms of
278 geological, hydrological, or biogeochemical parameters. Although geophysical data can be
279 interpreted qualitatively (e.g. by locating contrasts in geophysical properties), by monitoring
280 dynamic processes (Johnson et al., 2012; Singha et al., 2015), or through combination with other
281 methods (e.g. Day-Lewis and Lane, 2004; Moysey et al., 2005; Huisman et al., 2010; Miller et al.,
282 2014), petrophysical relationships are commonly used. Petrophysical relations can be used in joint
283 inversions to relate two independent geophysical methods (e.g. Hoversten et al., 2006; Zhang and
284 Revil, 2015) or after geophysical inversion to translate geophysical data. Although mechanistic
285 models exist (e.g. Leroy and Revil, 2009; Montaron, 2009, Revil et al., 2012), the majority of
286 petrophysical models used are semi-empirical or empirical. For instance, models have been
287 developed to relate electrical conductivity and porosity (Archie et al., 1942; Waxman and Smits,
288 1962), to link water content with dielectric permittivity (Topp et al., 1980), to interpret and IP
289 responses with surface area, grain size, and permeability (Vinegar and Waxman, 1984; Börner and
290 Schön, 1991; Slater and Lesmes, 2002; Binley et al., 2005; Slater et al., 2007; Weller et al., 2013;
291 2015a, b, c). It is also important to note that temperature has significant influence on electrical
292 conductivity, and as a result, ERI monitoring studies are often corrected for temperature (e.g. Brunet
293 et al 2010; Chambers et al 2014a; Uhlemann et al., 2016).

294 4. Geophysical characterisation of groundwater-surface water interactions

295 Geophysical applications to characterise properties and processes at the GW-SW interface can be
296 split into three principle areas: (1) characterising subsurface structure, (2) mapping zones of GW-SW
297 connectivity, and (3) monitoring hydrological processes. Whereas structural characterisation and
298 GW-SW exchange mapping have included studies at site and catchment scales, monitoring dynamic
299 processes has been conducted solely at site scales. In this section various geophysical applications
300 relevant to characterising the GW-SW interface are discussed. The majority of studies have focused

on freshwater streams and rivers; however, studies have also been conducted in wetlands, deltas, and lakes.

4.1. Structural characterisation

Structural characterisation is essential as the structure governs hydrological properties and subsequent processes. Although minimally intrusive, calibration of geophysics with intrusive methodologies is often required to interpret geophysical information (e.g. Zhou et al., 2000; Chambers et al., 2014b). Also, in some cases borehole methods involving ERT, IP, GPR, or seismic methods may be used for increased resolution of the deeper subsurface (e.g. Slater et al., 1997; Huisman et al., 2003; Kemna et al., 2004; Crook et al., 2008; Dorn et al., 2011). Nonetheless, geophysical methods provide a level of resolution that would be unachievable through use of point measurements alone.

4.1.1. Small scale structural characterisation

Several applications have used geophysics to characterise subsurface structure at the Hanford Nuclear Site (Washington, US) to assess pollution pathways to the Columbia River (Johnson et al., 2015). For example, Slater et al. (2010) used waterborne ERI and IP surveys to determine the contact depth of a high permeability unit and low permeability sections of the underlying unit. Depressions in the contact interface were interpreted to be palaeochannels, and were shown to be areas of GW discharge by using distributed temperature sensing. Land-based IP surveys were also conducted at the site and were effective in revealing contrasts between the two units and locating palaeochannels (Mwakanyamale et al., 2012). The locations of these palaeochannels were also in agreement with later studies that used temporally distributed ERI to monitor GW-SW interactions (Johnson et al., 2012; Wallin et al., 2013) as discussed in section 4.3. Also at the Hanford Site, Williams et al. (2012a-d) used seismic surveys over several tens of kilometres to interpolate the sandstone-basalt interface

between boreholes. They identified significant lows in the contact and determined additional potential pollution pathways to the Columbia River.

A number of geophysical studies have also been conducted at a riparian wetland (Boxford, UK). Crook et al. (2008) used surface and down borehole ER methods to reveal geological boundaries beneath the neighbouring River Lambourn. In the wetland, Chambers et al. (2014b) used ERI, soil probing and borehole data to characterise the 3D structure of the subsurface. They identified different superficial deposits, determined the depth to the chalk bedrock, and identified the weathering profile within the chalk, all of which are likely to have important hydrological implications (Figure 2). Loke et al. (2015) compared a standard ERI Wenner array and an optimised array and found that the optimised array was able to locate geological interfaces with greater accuracy. In another study, surface GPR revealed that the gravels subdivide into a lower section of chalky gravels and an upper section of coarse flint gravel (Newell et al., 2015). The study also found that gravels below a depth of 2 m were relatively structureless whereas the shallower gravels displayed potential point bar lateral accretion surfaces in association with the peat channels. The deposit architecture and the presence of low permeability weathered chalk are likely to have important implications for the hydrology of the site, with the superficial deposits perhaps creating direction dependent permeability.

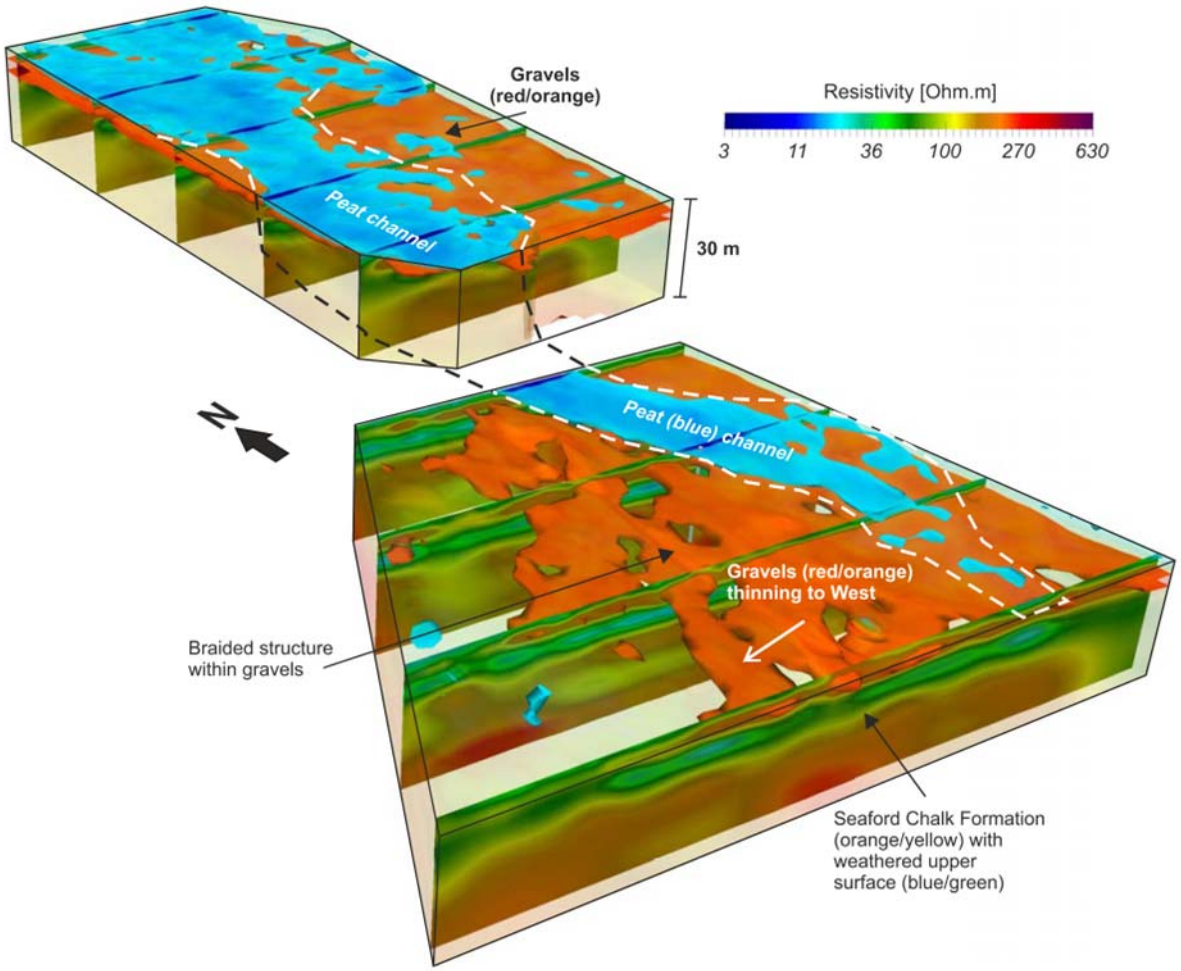

341

342 Figure 2: 3D resistivity model of the Boxford riparian wetland. Solid volumes are shown for regions
343 with resistivities of less than 50 Ohm.m in blue (peat) and with resistivities greater than 150 Ohm.m
344 in orange (gravel) (Chambers et al., 2014b).

345 Geophysics has also been employed successfully for site scale structural characterisation in a variety
346 of other settings. Crook et al. (2008) used ERI to evaluate the structure and volume of alluvial
347 deposits in Oregon (US), highlighting how it could be used to provide valuable information to model
348 biogeochemical exchange. In comparison, Mermillod-Blondin et al. (2015) characterised alluvial
349 structure using GPR in the Rhone River (Lyon, France). They identified two lithofacies and installed
350 piezometers to monitor hydraulic head and temperature. Samples were also taken to assess water
351 chemistry, sedimentology, and bacterial and invertebrate assemblages. They found that HEFs were
352 faster in the cobble/gravel facies than the gravel/sand facies, and that faster flow led to a greater

353 delivery of organic carbon and an increase in microbial activity. Revil et al. (2005) demonstrated how
354 ERI can be used to determine the 3D geometry of a palaeochannel and show that SP can be used to
355 determine preferential flow paths (Camargue, France). As well as constraining geological boundaries,
356 geophysics has been used to enhance the spatial extent of hydrological information. For example,
357 Miller et al. (2014) used ERI and permeameters to characterise broad scale hydrological patterns in
358 several alluvial floodplains in Oklahoma, US. Several studies have also indicated how multiple
359 geophysical techniques can be used to more accurately characterise the subsurface structure (e.g.
360 Gallardo and Meju, 2004; Günther and Rucker, 2006; JafarGardomi and Binley, 2013). For instance,
361 Doetsch et al. (2012a) and Zhou et al. (2014) were able to improve structural characterisation at the
362 Thur River, Switzerland by structurally guiding ERI inversion with GPR data.

363 Although the majority of structural studies provide static images of the system, SW systems,
364 particularly rivers, are characterised by dynamic erosional and depositional patterns. This dynamic
365 nature is known to have important hydrological and biogeochemical implications for processes in
366 the GW-SW interface (Elliot and Brooks, 1997; Packman and MacKay, 2003; Harvey et al., 2012).
367 Although the dynamic nature of the GW-SW interface has not been investigated using geophysics,
368 these issues are also important in civil engineering applications. The modification of flow velocities in
369 rivers due to bridges can lead to scouring and undermining of foundations (Anderson et al., 2007).
370 Several methods (e.g. echo sounding, intrusive measurements, bulk electrical conductivity probes)
371 have been used to assess changes in channel bed geometry (Prendergast and Gavin, 2014).
372 However, GPR and seismic methods have been particularly useful as they can provide information
373 about the channel geometry and sediment structure beneath the sediment-water interface without
374 the need for intrusive measurements (Webb et al., 2000; Prendergast and Gavin, 2014).

375 *4.1.2. Large scale structural characterisation*

376 Large scale structural characterisation has typically used airborne TD-EMI (AEM) in association with
377 other data sets. Harrington et al. (2014) used AEM, geological maps, and environmental tracers to

infer aquifer architecture beneath a large river in north-western Australia at the catchment scale (Figure 3). They postulated zones of GW discharge which could be useful in targeting sites for future investigation. AEM has also been used alongside geological mapping data to reveal sedimentary structures and faults (Jørgensen et al., 2012), with ERI to reveal geological variability in deltaic deposits (Meier et al., 2014), with borehole data to identify hydrofacies in glacial deposits (He et al., 2014), with seismic reflection to identify the bedrock-superficial interface (Oldenborger et al., 2016) and with modelling to aid in predicting nitrate reduction at catchment scales (Refsgaard et al., 2014). Although AEM dominates regional scale geophysical surveys, other techniques have also been used. Froese et al. (2005) used ERI and GPR at 20 to 40 km intervals, along with lithological descriptions of bank cuttings to characterise alluvial deposits along a 1000 km reach of the Yukon River (N. America), and Ball et al. (2006) used waterborne ERI and geological borehole data to characterise leakage potential in the Interstate and Tristate Canals (US). Columbero et al. (2014) also used waterborne ERI surveys to characterise the structure of a glacial lake (NW Italy). They identified an area where the lake silts had reduced thickness, and found that this region coincided with anomalous SP signals. They tentatively suggest SP can be used to locate zones of GW discharge.

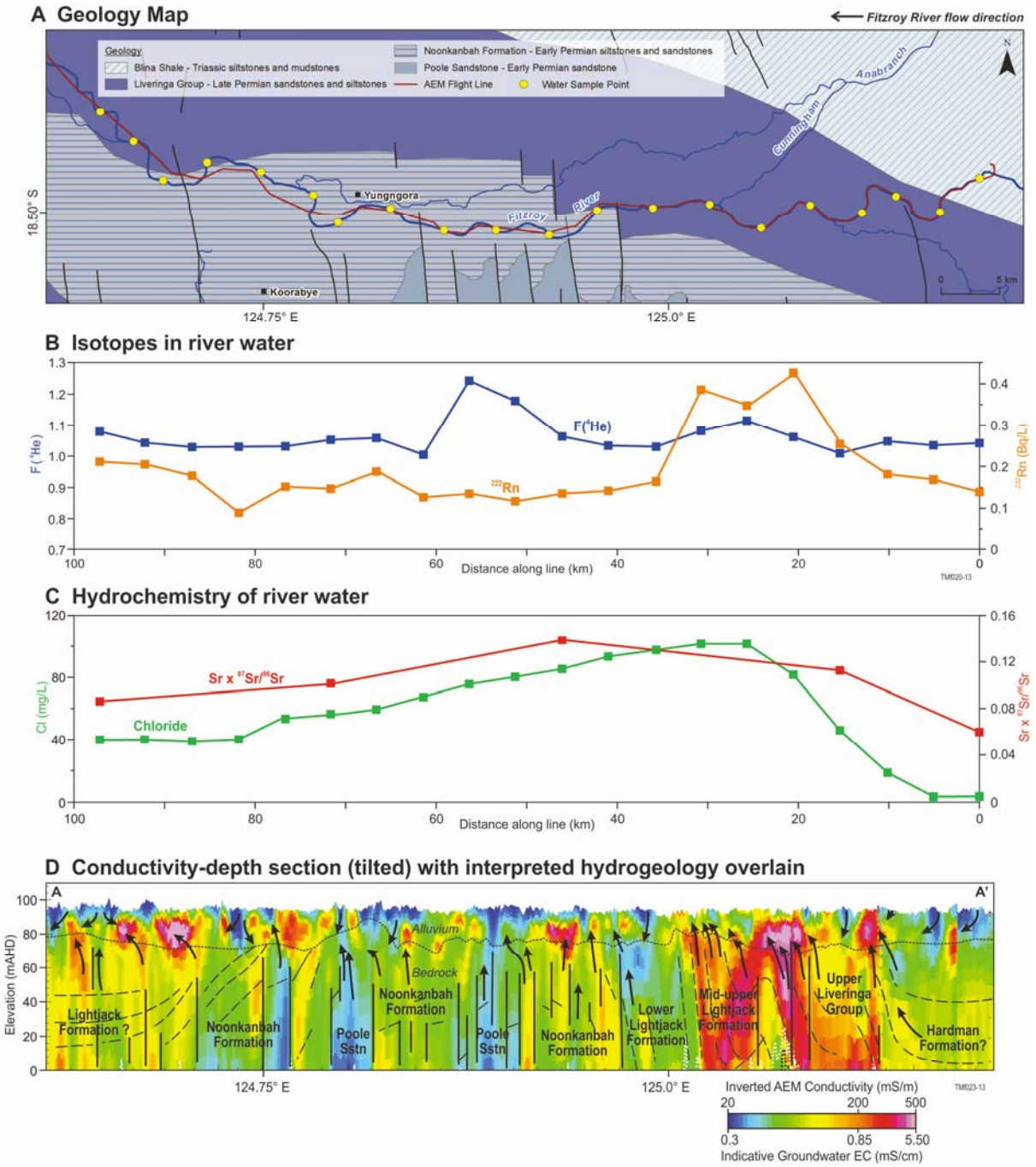

393

394 Figure 3: Combined plot showing (A) river water sample locations and AEM survey line with respect
395 to basement geology, (B) isotope data, (C) chemical data, and (D) an inverted conductivity-depth
396 section with litho-stratigraphic interpretation along AEM flight path, as shown in (A). Solid black lines
397 in (A) and (D) represent faults, dashed lines and arrows in (D) represent interpreted lithological
398 boundaries and groundwater flow directions. The conductivity-depth section is vertically
399 exaggerated with a V:H ratio of 1:100 (Harrington et al., 2014).

400 ### 4.2. Mapping zones of groundwater-surface water exchange

401 A principle consequence of structural heterogeneity is that it generates variability in GW-SW
402 connectivity. Identification of zones of enhanced GW-SW connectivity is important for informing
403 water management and locating areas of potential environmental significance (Buss et al., 2009;
404 Binley et al., 2013). Methods for assessing spatial variability in GW-SW exchange (e.g. seepagemeters
405 and piezometers) can be labour intensive to install. Several geophysical applications have
406 demonstrated how geophysics can exploit the contrasts in electrical and thermal properties of SW
407 and GW to identify areas of GW-SW interaction at site to catchment scales more quickly. In this way
408 geophysics can be used as a reconnaissance tool for identifying important areas for further study or
409 as an additional data source to extrapolate information between traditional measurements.

410 #### *4.2.1. Local scale mapping of groundwater-surface water interactions*

411 Although contrasts in the electrical properties of GW and SW are relatively small in freshwater
412 environments, several geophysical studies have been successful in revealing areas of GW-SW
413 exchange. For instance, Mansoor et al. (2006; 2007) used waterborne ERI to detect locations of
414 elevated pore water conductivities within an urban wetland which arose due to leaching from
415 marginal landfill sites during rainfall events. Nyquist et al. (2008) mapped locations of GW-SW
416 exchange within a stream section at metre-scale resolution by comparing 2D ERI sections collected at
417 high and low stage. Differences in the inverted models were interpreted as zones of GW-SW
418 exchange; these zones correlated with the thinning of a clay layer located beneath a carbonate
419 aquifer and the overlying alluvium. FD-EMI methods have also been used to reveal contrasts in
420 electrical conductivity and locate zones of GW-SW connectivity. Butler et al. (2004) used FD-EMI and
421 seismic methods to locate a clay aquitard and the extent of a clay window recharge zone. Binley et al.
422 (2013) used waterborne FD-EMI surveys alongside piezometric data and chemical sampling (Heppell
423 et al., 2014) to reveal spatial variability in GW discharge. Areas of high electrical conductivity were

correlated with upwelling of more solute rich GW, while areas of low electrical conductivity coincided with areas exhibiting horizontal hydraulic gradients (Figure 4).

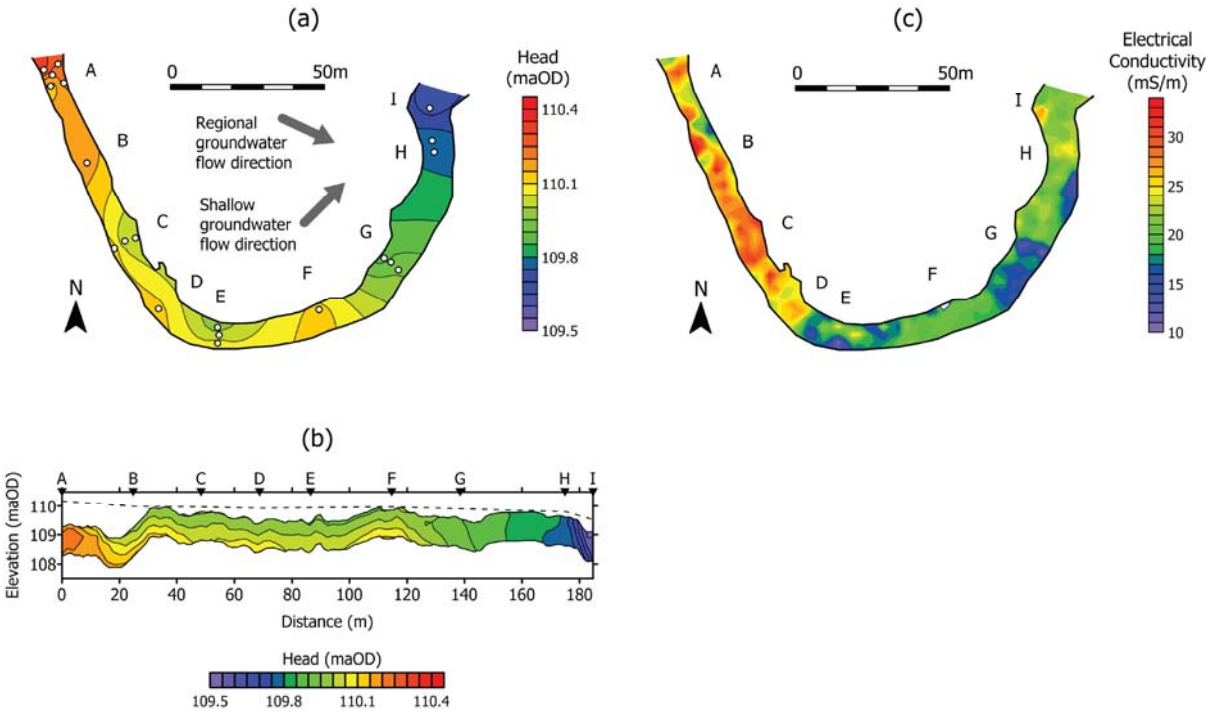

Figure 4: Comparison of interpolated hydraulic heads obtained from piezometers and electrical conductivity obtained from waterborne FD-EMI survey. (a) Horizontal profile obtained from 100 cm deep piezometers. Symbols show measurement locations. (b) Vertical profile obtained from 20, 50, and 100 cm deep piezometers. The dashed line shows measured stage profile. (c) Map of river bed electrical conductivity obtained using Geonics EM38. Hydraulic heads are shown in metres above ordinance datum (metres above sea level) (after Binley et al., 2013).

Contrasts in electrical conductivity have also been used in coastal environments where the contrasts can be much larger. For instance, Zarroca et al. (2014) used ERI methods in association with piezometric and natural tracer data in a coastal wetland. They were able to identify zones of focused upwelling and distinguish between local and regional GW flow paths, and the intrusion of seawater which converged in the wetland. Kinnear et al. (2013) demonstrated that FD-EMI could be used to

map lateral variability in electrical conductivity. They found that fresh GW discharge in the brackish Ringkøbing Fjord (Denmark) was constrained to the shoreline and demonstrated the potential for geophysical techniques to aid in assessing water budgets over large areas.

4.2.2. Catchment scale GW-SW connectivity mapping

In a similar way as structural characterisation, there have been several applications to map GW-SW connectivity at larger scales (hundreds of metres to tens of kilometres). Paine (2003) used field based FD-EMI to determine ranges in electrical conductivity and AEM to locate salinisation sources, in addition to quantifying lateral extent and intensity of salinitisation, by developing relationships from borehole water samples in northern Texas (US). In the Venice Lagoon (Italy), Viezzoli et al. (2010) used AEM to assess saltwater intrusion in the coastal aquifer and to characterise the transition between freshwater saturated sediments and overlying saltwater saturated sediments beneath the lagoon. Kirkegaard et al. (2011) used AEM in the Ringkøbing Fjord (Denmark) finding that buried valleys beneath the lagoon were characterised by high salinity waters while some areas of the lagoon were characterised by fresher waters. In the same fjord, Kinnear et al. (2013) used waterborne EMI surveys to reveal localised groundwater discharge zones into the brackish lagoon. ERI has also been used to map locations of GW-SW discharge. Kelly et al. (2009) used a towed waterborne ERI array and tracer data to differentiate between local and regional GW discharge along a 50 km river reach in South East Australia.

4.3. Monitoring groundwater-surface water interactions

In addition to using contrasts in the geophysical properties of GW and SW to map areas of exchange, geophysical techniques have been used to monitor and quantify processes of the GW-SW interface at local scales (metres to tens of metres). Aside from heat tracing methods, geophysical monitoring studies have almost exclusively involved ERI. However, Christiansen et al (2011) demonstrate how time-lapse gravity measurements can be used assess river-riparian zone exchanges. ERI methods are

somewhat analogous to monitoring wells in tracer experiments in that changes in resistivity are used to infer changes in hydrological properties or conditions (e.g. saturation or pore water conductivity). ERI can be used to image the entire region immediately beneath an electrode array. This means that low mobility zones, which are likely to be important in biogeochemical cycling, can be also be detected (Singha et al., 2008; Toran et al., 2013b).

Temporally distributed ERI surveys have been used at the Hanford Site (US) to monitor inland water intrusion in relation to changes in river stage and to detect high and low mobility zones in the riparian zone (Johnson et al., 2012; Wallin et al., 2013). They used time-series and time-frequency analysis to reveal the timing and location of GW-SW interactions. Cardenas and Markowski (2011) imaged a flood cycle in a dam regulated river finding that the HZ was laterally discontinuous and varied with time. In addition to surface electrodes, cross borehole ERI has been used to increase sensitivity at depths and locate areas of high and low permeability by monitoring 3D hydrological processes within the riparian zone of the Thur River, Switzerland (Coscia et al., 2011, 2012). At the Boxford riparian wetland, Uhlemann et al. (2016) found that peat exhibited a two layer behaviour separate by an intermittent clay layer; the upper layer showed a reduction in resistivity during the summer due to increased pore water conductivity and the lower layer exhibited an increase in resistivity during the winter months due to the reception of resistive GW.

Studies in fresh water environments have also used salt tracers to artificially induce electrical conductivity contrasts. For instance, Ward et al. (2010a) estimated the relative areas of the HZ by comparing a pre-injection ER model with subsequent post-injection ER models (Figure 5). More recently, Ward et al. (2013) monitored changes in the HZ finding that hydraulic gradients parallel and perpendicular to the valley gradient had minimal influence on HZ extent and that the HZ extent increased with decreasing vertical gradients away from the stream. Toran et al. (2012) compared ERI data from before and after installation of a restoration structure; they found that the HZ immediately upstream remained fairly constant but the HZ downstream decreased due to erosion and increases in

fine sediments. Similarly, Toran et al. (2013a) found that persistence of the saline tracer was more dependent on thickness and grain size rather than on the presence of restoration structures. Recently, Houzé et al. (2017) used a 3D array to obtain 7 m x 1 m x 1 m resistivity images of the subsurface following the injection of a tracer into the subsurface and note the importance of characterising boundary conditions for inverse modelling.

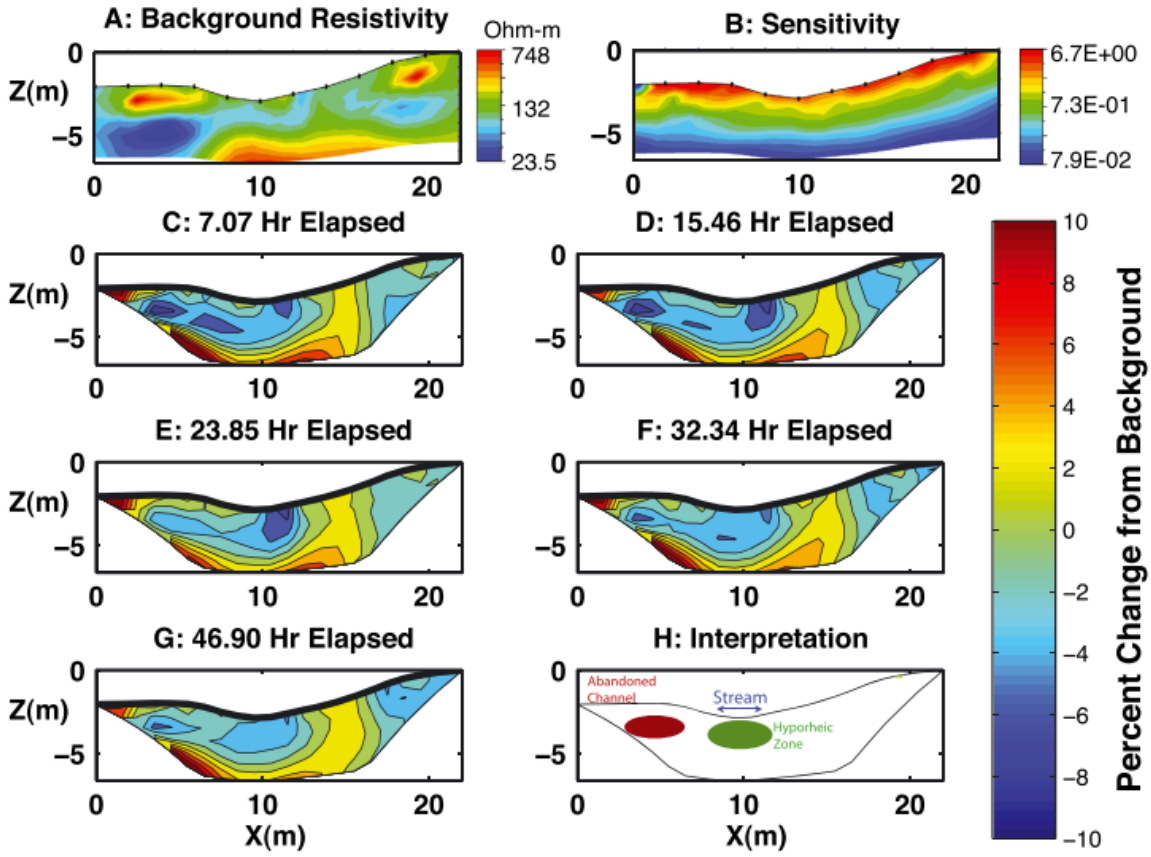

Figure 5: Electrical resistivity imaging of solute transport in subsurface of a stream during a 21 hour injection. Transects run perpendicular to the stream, with flow direction out of the page. (A) Pre-injection electrical resistivity model. (B) Model sensitivity based on the positions of electrodes in the electrode array. (C-G) Time-lapse ERI results, at time elapsed after beginning the conservative solute injection. Colour indicates percentage change in bulk resistivity from background conditions. (H) Interpretation of resistivity images. Resistive feature in pre-injection model is interpreted to be an abandoned cobble bed (Singha et al., 2015; adapted from Ward et al. 2010a).

ERI and salt tracer studies have also been used to monitor processes in the riparian zone. To investigate the importance of voids in the riparian zone Menichino et al. (2014) created an artificial macro-pore and monitored intra-meander flow using ERI. They found that their open macro-pore enabled more solute transport and increased solute tailing, both of which are likely to be important in hydrological and biogeochemical processes. Whereas Doetsch et al. (2012b) used a 3D ERI monitoring array to estimate riparian zone infiltration velocities and found agreement with monitoring well data.

Similar to mapping zones of exchange, the natural conductivity contrasts in coastal environments can be used to monitor GW-SW interaction processes. Swarzenski et al. (2007) investigated bidirectional exchange between a coastal aquifer and sea water using ERI, electromagnetic seepage meters and geochemical tracers. They found that the tide strongly influenced hydraulic gradients such that during high tides GW discharge was reversed and sea water infiltrated into the coastal aquifer. In a similar experiment, Henderson et al. (2010) found that their ERI also indicated suppressed GW discharge, whereas temperature measurements indicated GW discharge continued at high tide. Their sensitivity modelling indicated that during high tide electrical current was preferentially focused in the conductive SW and that consequently, the resistive GW could not be easily resolved. This demonstrates the issue of method sensitivity to the chosen set up or environment, and also highlights the importance of forward modelling to realise the sensitivity of geophysical data.

5. Discussion

Geophysical techniques have successfully provided information about processes and properties relevant to the GW-SW interface, with research focusing on three key areas: (1) characterising structure, (2) mapping zones of GW-SW interaction, and (3) monitoring dynamic processes. However, studies of properties and processes in the GW-SW interface would benefit from continued geophysical input, for which there are several avenues of potential research. In this section the

strengths, challenges, and recent developments in geophysical techniques are discussed alongside opportunities for the future.

5.1 Strengths of geophysics

It is convenient to organise geophysical techniques into more general themes to consider their strengths as tools to: (1) guide more focused investigations, (2) supplement other data sets, and (3) monitor dynamic processes. These strengths are also apparent in other fields of near surface geophysics (e.g. Singha et al., 2015; Binley et al., 2015; Parsekian et al., 2015). Their presence highlights the scope of geophysics for studies concerned with the GW-SW interface and more general environmental applications.

5.1.1. Reconnaissance tools

Often the usefulness of data can only be appreciated following the instrumentation of a site. By targeting specific sites based on preliminary geophysical investigations it may be possible to save resources and obtain more representative and useful information. In addition, at catchment scales the decision to select a particular site may be purely incidental to land access and prior instrumentation. At local scales FD-EMI (e.g. Butler, et al. 2004; Binley et al., 2013) and ERI (e.g. Mansoor and Slater, 2007; Nyquist et al., 2008) have been shown to be capable of identifying zones of hydrological interest. However, geophysics has also been used to locate areas of biogeochemical interest. For example, Uhlemann et al. (2017) used ERI to guide biogeochemical and hydrological sampling of an arsenic contaminated aquifer in Cambodia (Richards et al., 2017) by characterising its sedimentological setting. In this way, geophysics can also be used to improve the confidence that intrusive data is representative or appropriate for characterisation of the site.

Additionally, geophysics has also been used as a reconnaissance tool at catchment scales; AEM has been used for locating palaeochannels (Worrall et al., 1999; Abraham et al., 2012) and areas of GW-SW connectivity (Jørgensen et al., 2012; Harrington et al., 2014). As noted by Kruse (2013), there is

550 significant potential for combining remote sensing data with aerial and land based geophysics. These
551 methods are highly complementary given that remote sensing data is typically sensitive to the
552 shallow subsurface (<1 m) whereas geophysical techniques may be sensitive up to depths of several
553 tens or hundreds of metres (Parsekian et al., 2015). Geophysics and remote sensing has been
554 combined in permafrost studies, for instance AEM (Pastick et al. 2013) and ground based ERI and
555 GPR (Yoshikawa and Hinzman, 2003) was used to assess the thickness and distribution of permafrost.
556 Approaches such as those employed by Wilson et al. (2016), whereby lakes were prioritised based on
557 their geological setting before thermal imagery was analysed, could be enhanced by inclusion of
558 geophysical data. The combination of remote sensing data and geophysics would be useful in linking
559 surface and subsurface properties and would be a powerful tool in GW-SW interaction studies.
560 Furthermore, these applications could provide additional constraints for catchment scale
561 considerations of HEFs (e.g. Kiel and Cardenas, 2014; Gomez-Velez and Harvey, 2014).

562 *5.1.2. Supplementing other data sets*

563 Geophysical measurements that are sensitive to geological, hydrological or biogeochemical
564 properties can be used to reduce interpolation uncertainty and increase the spatial coverage of
565 information. The combination of methods has additional advantages in that by combining different
566 data sources, poor sensitivity and other methodological limitations can be reduced. Combining data
567 sets is common in GW-SW interface research. For instance, González-Pinzón et al. (2015) combined
568 centimetre scale probes with chemical tracers, piezometers, fibre-optic distributed temperature
569 sensing, temperature sensors and electrical resistivity imaging to improve conceptual understanding
570 of a river reach at several scales. The development of integrated and standardised approaches may
571 also be beneficial for generating common data sets to compare field sites and improve conceptual
572 models. Multi-method approaches are similarly used in hydrogeophysical research to combine
573 geophysical techniques with hydrological and geophysical techniques (e.g. Moyse et al., 2005; Hinnel
574 et al., 2010). The grouping of traditional and geophysical applications can improve the spatial extent

575 of available information across a range of scales and improve the quantative interpretation of
576 geophysical data. To date most geophysical studies of the GW-SW interface have focused on
577 characterising the geological structure. Future applications should endeavour to extract information
578 about the hydrological and biogeochemical properties of the subsurface.

579 *5.1.3. Monitoring dynamic processes*

580 Processes occurring at the GW-SW interface can be highly dynamic. It can be difficult to characterise
581 these processes with traditional methods as they can interrupt processes and continuous
582 measurements may not be possible. In this review, the ability of ERI to characterise dynamic
583 processes has been demonstrated (e.g. Ward et al., 2010a; Johnson et al., 2012; Wallin et al., 2013).
584 These strengths are also highlighted in related fields where ERI and IP have been used to monitor
585 contaminant transport, biological activity and biogeochemical processes (e.g. Michot et al., 2003;
586 Garre et al., 2011; Slater and Atekwana., 2009; Johnson et al., 2010; Flores Orozco et al., 2011; Chen
587 et al., 2012; Singha et al., 2015). It is anticipated that knowledge from these fields could be applied to
588 characterisation of the GW-SW interface. In addition, temporally distributed surveys of other
589 geophysical methods may be beneficial, for example FD-EMI could be used to extend the information
590 obtained in ERI monitoring studies and temporally distributed GPR, or seismic, surveys could be used
591 to better characterise the dynamic nature of river bed geomorphology.

592 ## 5.2. Challenges of geophysics

593 Despite the progress made by geophysics it is also important to appreciate the challenges of
594 geophysical methods. These are related to geophysics in general and are on-going issues in
595 geophysical research. The principal challenges of geophysical techniques are that: (1) geophysics is
596 inherently uncertain, (2) site specific considerations are often needed, and (3) geophysics needs to
597 be processed and modelled for quantitative interpretation. These limitations greatly contribute to
598 the reluctance to adopt geophysical techniques in environmental studies. Here these challenges are

599 discussed briefly but it is anticipated that by addressing the issues more thoroughly, application of
600 geophysics in environmental sensing will become more common.

601 *5.2.1. Geophysical uncertainty*

602 Geophysical data and modelling methods are uncertain. Despite the broad recognition of errors in
603 geophysical methods, they can be poorly dealt with and as a result, incorrect interpretations of
604 geophysical data can be made (Binley et al., 2015). For instance, GPR and EMI survey devices often
605 need to be corrected for instrument drift (Jacob and Hermance, 2004; De Smedt et al., 2016).
606 Particular interest has been given to errors in ERI data. Typically, stacked or reciprocal measurements
607 are used to assess the quality of measurements and weight them appropriately in inverse modelling
608 (Binley, 2015; Singha et al., 2015). Stacked errors are obtained from consecutive repeat
609 measurements for each current injection and reciprocal errors are obtained by reversing the
610 measurement sequence and conducting a second survey. Reciprocal measurements are typically
611 viewed as being more robust, as stacked measurements may underestimate measurement error (Tso
612 et al., in review). However, it should be noted that if the process of interest is occurring faster than a
613 direct and reciprocal measurement scheme, then reciprocal errors may not be so useful (e.g. Ward et
614 al., 2010a). Additionally, some studies have also looked at assessing the value of information in
615 geophysical images in order to assess how reliable geophysical models are (e.g. Oldenburg and Li,
616 1999; Daily et al., 2005). For instance, Oldenburg and Li (1999) use a depth of investigation method
617 to assess the vertical reliability of ER and IP models. More recently, JafarGardomi and Binley (2013)
618 investigated the information content of combined ERI, FD-EMI and GPR data sets, and Nenna and
619 Knight (2013) assessed the benefit of adding geophysical data to assess maintenance of a coastal
620 aquifer. Methods similar to these could assist in determining the value of data assimilation and help
621 to aid in survey design.

622 *4.2.2. Site specific considerations*

In all applications, it is important to consider the target, scale of interest and the likely subsurface properties in order to return the most beneficial information. For instance, larger electrode spacing in ERI and IP or lower frequencies in GPR surveys will permit characterisation to deeper depths, but will sacrifice resolution (Binley et al. 2015; van der Kruk et al., 2015). Forward modelling tools such as Terry et al. (2017) can help to guide survey design based on the targets of interest and the expected subsurface properties. In some cases, geophysical surveys may be optimised, for example in ERI electrode number, position and measurement geometry can be designed to improve spatial resolution whilst removing unnecessary measurements and consequently reducing measurement time (Wilkinson et al., 2006; 2012; Loke et al., 2015).

It is useful to briefly note some of the considerations necessary to applications in SW bodies. The water column can be problematic as it can create current focusing effects in methods influenced by electrical conductivity (e.g. ERI, IP, EMI and GPR). For instance, in ERI of river beds the depth of investigation required, the river level, and electrical conductivity of river water should be taken into consideration when deciding the electrode spacing and whether to use floating arrays or bed electrodes (Snyder et al., 2002). These measurements can also aid in interpretation of data (e.g. Slater et al., 2010; Binley et al., 2013). However, it should be noted that additional constraints make it more difficult to solve inverse problems and errors in measurements of water depth or in-stream electrical conductivity may lead to significant inversion artefacts (Day-Lewis et al., 2006). ERI studies in SW bodies have involved static arrays (Nyquist et al., 2008; Crook et al., 2008) and towed arrays (e.g. Kelly et al., 2009; Slater et al., 2010). The latter methodology has benefits in that it can improve survey productivity; however, it precludes error quantification (Slater et al., 2010) and requires various electrode spacings to improve vertical resolution (Allen, 2007). In addition to resolution and methodology considerations, some geophysical applications may not be appropriate for the setting. For example, use of salt tracers and ERI may be prohibited in ecologically sensitive areas, or GPR signals may be attenuated in highly electrically conductive areas.

5.2.3. Extracting quantitative information

Recovering quantitative information from geophysics is a major challenge and has been the subject of numerous reviews (e.g. Rubin and Hubbard, 2005; Singha et al., 2007; 2015; Loke et al., 2013). Hydrogeological information can be extracted from geophysical data by using petrophysical relationships, interpreting time-lapse data and through combination with other techniques. Petrophysical models are commonly used due to their simplicity; however, their usage can be problematic. As noted by Singha et al. (2015) translation of geophysical images with poorly resolved heterogeneity or inversion artefacts will be erroneous, the support volumes of geophysical and hydrological parameters are often different, meaning conversions can be poor, and the resolution of geophysical images can be spatially and temporally variable such that petrophysical transformations may be inconsistent. Geophysical information can also be interpreted temporally without the need for petrophysical transformations. Johnson et al. (2012) and Wallin et al. (2013) used time-series and time-frequency analyses of the Columbia River stage and ERI to reveal preferential pathways, whereas Ward et al. (2010b) demonstrated that temporal moments of ER and solute transport data were well correlated for diffusive transport in the HZ. Geophysical data may also be interpreted from the combination with other techniques. For example, calibrating geophysical and hydrological data at point scale and estimating the correlation at field scale (Day-Lewis and Lane, 2004), by using changes in geophysical properties to calibrate hydrological models (e.g. Binley et al., 2002), or by coupled (e.g. Hinnel et al., 2010) and joint inversions (Kowalsky et al., 2005; Johnson et al., 2009).

As noted, many applications to characterise the structure of the GW-SW interface (i.e. static surveys) have been qualitative in that they are used to reveal geometry of geological deposits. Future applications should aim to characterise properties such as permeability, surface area and cation exchange capacity. Although petrophysical models are often used to translate static geophysical data following inversion, in recent years there has been increasing interest in joint inversions. Joint inversions use petrophysical relations to link multiple geophysical data sets with each other, or with

673 hydrological data sets. They have demonstrated significant potential in recovering hydrological
674 properties (Kowalsky et al., 2005; Johnson et al., 2009; Jardani et al., 2013; Soueid Ahmed et al.,
675 2014; 2016) and are a promising direction for quantative interpretation of geophysical surveys of the
676 GW-SW interface.

677 ## 5.3. Recent developments in geophysical applications

678 Since the advent of hydrogeophysics during the 1990s (Binley, 2015), geophysical techniques have
679 evolved from their traditional exploratory usage to being capable of characterisation of hydrological
680 states and dynamic processes. Additionally, in more recent years the field of biogeophysics, which
681 aims to relate the biological processes and modifications of the subsurface to geophysical properties,
682 has emerged (Atekwana and Slater, 2009). Biogeophysical applications have typically involved
683 characterising reactive conditions (e.g. Naudet et al., 2003; Sassen et al., 2012; Chen et al., 2013),
684 detecting biogeochemical by-products (e.g. Slater and Binley, 2006; Comas et al., 2007; 2014;
685 Parsekian et al., 2011), or detecting changes to physical structure as a result of microbial activity (e.g.
686 Williams et al., 2005; Slater et al., 2008). In addition, the usage of unmanned vehicles in
687 environmental research has vastly increased and it is expected that automated deployment of
688 miniaturised geophysical devices could become common in future years. In this section
689 developments in: (1) electrical resistivity monitoring, (2) induced polarisation, (3) self-potential, (4)
690 multi-coil electromagnetic induction, and (5) automated vehicles and their potential application in
691 GW-SW characterisation are discussed.

692 ### *5.3.1. Electrical resistivity monitoring*

693 ERI is one of the most commonly and widely applied geophysical methods. There has been
694 significant interest in developing low power, automated instruments for long term monitoring (e.g.
695 Daily et al., 2004; Kuras et al. 2009; Ogilvy et al., 2009; Chambers et al., 2015). These instruments
696 have the potential to provide spatially extensive data sets, with high spatial and temporal resolution.

Moreover, instruments can also transmit data to high performance computers to allow for real time monitoring of subsurface processes (Singha et al., 2015). For instance, computational advances in inversion schemes, e.g. image differencing to avoid regularisation in the time dimension (Wallin et al., 2013) or parameterisation based on the physics of plume shape evolution (e.g. Miled and Miller, 2009; Pidlisecky et al., 2011), are promising tools for extracting hydrological information from ERI monitoring data. As noted, time-lapse ERI to monitor processes in the HZ typically do not use reciprocal measurements as a more robust estimate of error as acquisition times are perhaps too long for revealing processes of interest. ERI acquisition times could be reduced using multi-channel systems, optimised electrode arrays (e.g. Wilkinson et al., 2012), or shorter current injection. However, it should be noted that use of short injection times could result in unreliable measurements of resistivity (Binley, 2015). Also, although most studies have been conducted over periods of several hours, longer ERI monitoring studies such as that of Uhlemann et al. (2016) could be used to aid in revealing seasonal variation in GW upwelling or river-riparian zone interactions.

5.3.2. Induced polarisation

Despite being less commonly used than ERI, many modern ERI instruments are also capable of IP measurements. Although, ERI is more robust in that it has higher signal to noise ratios, the IP signal is more closely related to geological characteristics and petrophysical relationships exist for relating IP signal to surface area, permeability and cation exchange (Vinegar and Waxman, 1984; Börner and Schön, 1991; Slater et al., 2007; Revil et al., 2012; Weller et al., 2015). These properties have clear relevance to the GW-SW interface, however, IP studies of the GW-SW interface have been limited (e.g. Slater et al., 2010; Mwakanyamale et al. 2012). The limited application, in comparison to ERI, is probably due to the complexity associated with analysis of data and future applications should be cautious in interpretation of IP data. Nonetheless, it is anticipated that IP would be beneficial in revealing variability in permeability, surface area and cation exchange capacity, and potentially biogeochemical processes (e.g. Flores Orozco et al., 2011; Chen et al., 2012), at the GW-SW interface.

5.3.3. Self-potential

Similar to IP, usage of SP in GW-SW interaction studies has been less frequent; however, there are several possible applications. The SP signal arises from electro-kinetic, electro-chemical, and thermo-electric sources. SP has been used to characterise hydraulic conductivity during pumping tests (Rizzo et al., 2004; Revil et al., 2008; Soueid Ahmed et al., 2014; 2016), through palaeochannels (Revil et al., 2005), through fractures (Wishart et al., 2006; 2008), and in arctic hill-slopes (Voytek et al., 2016). Applications in GW-SW interface research could involve assessing the spatial and temporal variability of GW discharge (e.g. Colombero et al., 2014) or HEFs, or characterising hydraulic conductivity. However, perhaps the most intriguing use of SP at the GW-SW interface would be to characterise the variability in redox conditions. SP has been used to extend the spatial coverage of redox measurements obtained from monitoring wells associated with a contaminant plume at the Entressen Landfill in France (Figure 6) (Naudet et al., 2003; 2004; Arora et al., 2007; Linde and Revil, 2007). Naudet et al. (2004) removed the electro-kinetic contribution using piezometric head data and found that the SP signal and redox potential values showed good correlation ($R^2 = 0.85$). It is however important to note the differentiation of SP sources may be more complex in the GW-SW interface, and the electro-kinetic effect may dominate the signal. Any work involving SP would need to account for all sources of the SP signal appropriately in addition to adequate understanding of redox chemistry.

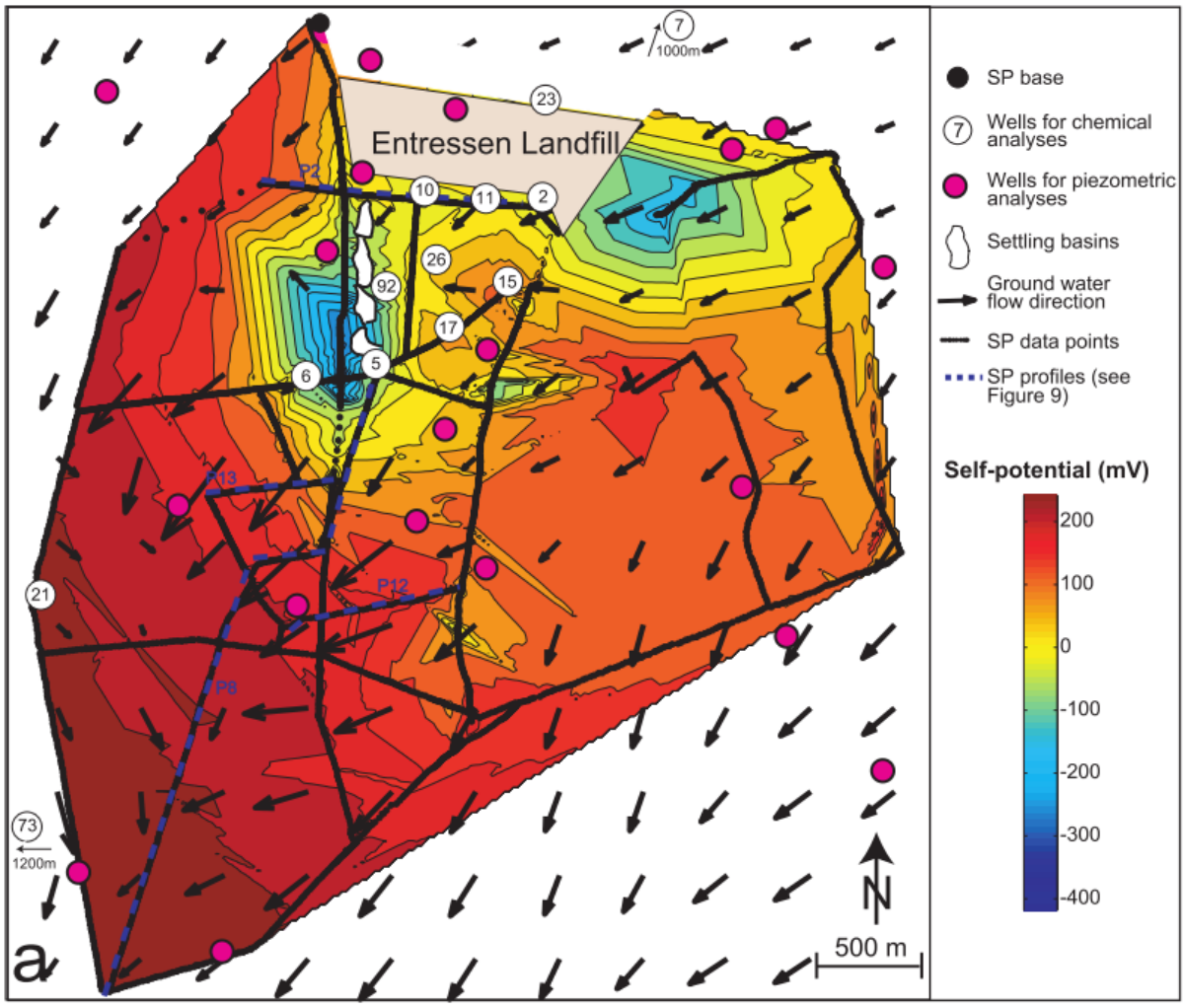

Figure 6: Map of self-potential obtained by linear interpolation of measurements made at 10 m resolution in first 2 km from landfill site and 20 m elsewhere. Hydraulic gradients obtained from piezometers (Naudet et al., 2004).

4.3.4. Multi-coil electromagnetic induction

In recent years FD-EMI instruments have been increasingly used in hydrological investigations due to their improved reliability and stability (Boaga, 2017). Furthermore, FD-EMI methods have the advantage over ERI in that they do not require contact with the ground and can therefore be more productive. Modern FD-EMI instruments contain multiple coils and are more easily able to provide information about vertical variability in addition to lateral variability. They therefore make it possible to extend the application of FD-EMI beyond qualitative mapping of GW-SW interactions (e.g. Butler

et al., 2004; Binley et al., 2013; Kinnear et al., 2013). In addition, as noted recently by Christiansen et al. (2016), the majority of studies present apparent electrical conductivity, e.g. without appropriate data processing or inverse modelling. Advances in data filtering and inversion schemes, such as EM4Soil (EMTOMO, 2013), Aarhus Workbench (Christiansen et al., 2016) or FEMIC (Elwaseif et al., 2017), permit more accurate modelling of subsurface conductivity structure and may lead to more reliable subsurface characterisation using FD-EMI

Furthermore, temporally distributed FD-EMI surveys similar Robinson et al. (2012), Shanahan et al., (2015) Huang et al., (2017) could prove useful in GW-SW interface characterisation. For instance, FD-EMI instruments could be used to investigate diurnal dynamics of salt water wedges in coastal environments or seasonal changes in GW upwelling, provided there are substantial contrasts in the electrical conductivity of GW and SW. It is important, however, to note that some authors (e.g. Lavoué et al., 2010) argue for the need to calibrate FD-EMI with ERI, this may be particularly true in time-lapse measurements where ambient conditions (e.g. air temperature), or the operator, may influence the readings obtained.

4.3.5. Unmanned vehicle based data acquisition

Given the significant increase in the availability and application of automated ground-based, waterborne and aerial technology in many aspects of environmental sensing, the translation to geophysical sensing is inevitable. Automated aerial, terrestrial and waterborne vehicles offer the ability for precise and repeatable data collection. Unmanned aerial vehicles have the ability to fly at lower elevations (~30 m) than typical aircraft, and are therefore able to provide high resolution data sets without sacrificing productivity. Geophysical applications using automated vehicles have predominantly involved magnetic mapping to locate manmade features (Stoll, 2013; Phelps et al., 2014). Automated vehicles may also be able to simultaneously process and contour data, and transmit information in real time (Phelps et al., 2014). Furthermore, automated systems could be

775 programmed in such a way that anomalous regions are re-surveyed in higher resolution
776 automatically.

777 The majority of unmanned aerial vehicles are small (<25 kg) and are limited to light weight
778 instruments, however larger vehicles capable of carrying heavier payloads are available (Whitehead
779 et al., 2014a, b). It can be envisaged that miniaturisation (or weight reduction) of geophysical tools,
780 and the increasing pay loads of UAVs, could allow for increased collection of automated aerial
781 geophysical data. However, non-aerial geophysical applications could easily be adapted to use
782 automated vehicles, for instance roving surveys using plate electrodes for ERI (Christensen and
783 Sørensen, 1998), large scale FD-EMI surveys (Christiansen et al., 2016) or waterborne surveys (Kelly
784 et al., 2009; Binley et al., 2013; Colombero et al., 2014) would not be difficult to automate and may
785 aid in collection of data across larger scale, e.g. to investigate parameters at catchment scales.

786 5. Summary

787 Geophysical tools have clear application in revealing geological, hydrological and biogeochemical
788 heterogeneity at the GW-SW interface. Geophysical tools are highly complementary to traditional
789 tools as they are sensitive to regions of the subsurface not reachable by direct measurements. The
790 majority of geophysical applications have focused on characterising subsurface structure, revealing
791 spatial variability in GW-SW interaction and imaging hydrological processes. Data sets obtained from
792 these field studies have significant potential to improve characterisation and modelling of
793 parameters at the GW-SW interface. Over the last 20 years geophysics has grown to be a powerful
794 tool in hydrogeological research, in part due to the view that geophysical tools be used to aid
795 hydrogeological problems alongside traditional methods. Geophysics provides valuable practical
796 tools for assessing many unknowns of the GW-SW interface. Moreover, although caution in
797 quantative interpretation of geophysical data is warranted, attempts at improving uncertainty
798 quantification, inversion routines and translating data are on-going. Efforts to provide solutions to
799 these issues can only continue to improve confidence in geophysics so that its potential can be more

widely appreciated and applied across a variety of scales. In recent years, there has been significant development in techniques and methodologies in parallel research areas, some of which would enhance the information obtained in studies of the GW-SW interface. Continued integration of geophysical methods would be beneficial in characterising hydrological and biogeochemical heterogeneity in the GW-SW interface and understanding the implications for water quality and ecological health.

Acknowledgements

We are grateful to André Revil, Kamini Singha and an anonymous reviewer for their comments on an earlier version of the manuscript. This work is supported by the UK NERC Envision Doctoral Training Programme (GA/15S/004 S301). The contributions of J. Chambers and S. Uhlemann are published with the permission of the Executive Director of the British Geological Survey (NERC).

References

Abraham, J. D., Cannia, J. C., Bedrosian, P. A., Johnson, M. R., Ball, L. B., Sibray, S. S. (2012). Airborne electromagnetic mapping of the base of aquifer in areas of western Nebraska. US Geological Survey Scientific Investigations Report 2011-5219, 1–38. https://pubs.usgs.gov/sir/2011/5219/

Allen, D. A. (2007). Electrical conductivity imaging of aquifers connected to watercourse. Faculty of Science, University of Technology, Sydney PhD Dissertation, 1–438.

Anderson, N. L., Ismael, A. M., & Thitimakorn, T. (2007). Ground-Penetrating Radar: A Tool for Monitoring Bridge Scour. Environmental & Engineering Geoscience. 13(1), 1–10. http://pubs.er.usgs.gov/publication/70031991

Annan, A. P. (2005). GPR methods for Hydrogeological Studies. In: Rubin, Y., Hubbard, S.S. (Editors) Hydrogeophysics. Netherlands: Springer. p185–213.

823 Archie, G. E. (1942). The Electrical Resistivity Log as an Aid in Determining Some Reservoir
824 Characteristics. Transactions of the American Institute of Mining and Metallurgical
825 Engineers, 146, 54–62. https://doi.org/10.2118/942054-G

826 Arora, T., Linde, N., Revil, A., & Castermant, J. (2007). Non-intrusive characterization of the redox
827 potential of landfill leachate plumes from self-potential data. Journal of Contaminant
828 Hydrology, 92, 274–292. https://doi.org/10.1016/j.jconhyd.2007.01.018

829 Aster, R., B. Borchers, & Thurbur, C. (2005). Parameter Estimation and Inverse Problems, 2nd Edition.
830 New York, US: Academic Press.

831 Atekwana, E. A., & Slater, L. D. (2009). Biogeophysics: A new frontier in Earth science research.
832 Reviews of Geophysics, 47, 1–30. https://doi.org/10.1029/2009RG000285

833 Ball, L. B., Kress, W. H., & Cannia, J. C. (2006). Determination of canal leakage potential using
834 continuous resistivity profiling techniques in western Nebraska and eastern Wyoming, 2004.
835 US Geological Survey Scientific Investigations Report 2006 -5032, 1–53.
836 https://pubs.water.usgs.gov/sir20065032

837 Bencala, K. E. (1984). Interactions of solutes and streambed sediment: 2. A dynamic analysis of
838 coupled hydrologic and chemical processes that determine solute transport. Water
839 Resources Research, 20(12), 1804–1814. https://doi.org/10.1029/WR020i012p01804

840 Bencala, K. E., Kennedy, K. C., Zellweger, G. W., Jackman, A. P., & Avanzino, R. J. (1984). Interactions of
841 Solutes and Streambed Sediment: 1. An Experimental Analysis of Cation and Anion Transport
842 in a Mountain Stream. Water Resources Research, 20(12), 1797–1803.
843 http://onlinelibrary.wiley.com/doi/10.1029/WR020i012p01797/full

844 Bianchin, M. S., Smith, L., & Beckie, R. D. (2011). Defining the hyporheic zone in a large tidally
845 influenced river. Journal of Hydrology, 406, 16–29.
846 https://doi.org/10.1016/j.jhydrol.2011.05.056

847 Binley, A., Cassiani, G., Middleton, R., & Winship, P. (2002). Vadose zone flow model parameterisation
848 using cross-borehole radar and resistivity imaging. Journal of Hydrology, 267(3–4), 147–159.
849 https://doi.org/10.1016/S0022-1694(02)00146-4

850 Binley, A., Slater, L. D., Fukes, M., & Cassiani, G. (2005). Relationship between spectral induced
851 polarization and hydraulic properties of saturated and unsaturated sandstone. Water
852 Resources Research, 41, W12417, 1-13. https://doi.org/10.1029/2005WR004202

853 Binley, A., Ullah, S., Heathwaite, L., Heppell, C., Byrne, P., Lansdown, K., Trimmer, M., & Zhang, H.
854 (2013). Revealing the spatial variability of water fluxes at the groundwater-surface water
855 interface. Water Resources Research, 49(7), 3978–3992. https://doi.org/10.1002/wrcr.20214

856 Binley, A. (2015). Tools and Techniques: Electrical Methods. In: Schubert, G. (Editor). Treatise on
857 Geophysics, 2nd Edition, Vol. 11. Oxford, UK: Elsevier. p233-259.
858 https://doi.org/10.1016/B978-0-444-53802-4.00192-5

859 Binley, A., Hubbard, S. S., Huisman, J. A., Revil, A., Robinson, D. A., Singha, K., & Slater, L. D. (2015).
860 The emergence of hydrogeophysics for improved understanding of subsurface processes
861 over multiple scales. Water Resources Research, 51(6), 3837–38366.
862 https://doi.org/10.1002/2015WR017016

863 Boaga, J. (2017). The use of FDEM in hydrogeophysics: A review. Journal of Applied Geophysics, 139,
864 36–46. https://doi.org/10.1016/j.jappgeo.2017.02.011

865 Boano, F., Revelli, R., & Ridolfi, L. (2008). Reduction of the hyporheic zone volume due to the stream-
866 aquifer interaction. Geophysical Research Letters, 35(9), L09401, 1–5.
867 https://doi.org/10.1029/2008GL033554

868 Boano, F., Harvey, J. W., Marion, A., Packman, A. I., Revelli, R., Ridolfi, L., & Wörman, A. (2014).
869 Hyporheic flow and transport processes: Mechanisms, models, and biogeochemical
870 implications. Reviews of Geophysics, 52(4), 603–679.
871 https://doi.org/10.1002/2012RG000417

872 Börner, F. D. & Schön, J. H. (1991). Technical note: A relation between the quadrature component of
873 electrical conductivity and the specific surface area of sedimentary rocks. Society of
874 Petrophysicists and Well-Log Analysts, 32(5), 612–613.

875 Boulton, A. J., Findlay, S., Marmonier, P., Stanley, E. H., & Valett, H. M. (1998). The Functional
876 Significance of the Hyporheic Zone in Streams and Rivers. Annual Review of Ecology and
877 Systematics, 29, 59–81. https://doi.org/10.1146/annurev.ecolsys.29.1.59

878 Boulton, A. J., Datry, T., Kasahara, T., Mutz, M., & Stanford, J. A. (2010). Ecology and management of
879 the hyporheic zone: stream–groundwater interactions of running waters and their
880 floodplains. Journal of the North American Benthological Society, 29(1), 26–40.
881 https://doi.org/10.1899/08-017.1

882 Bridge, J. W. (2005). High resolution in-situ monitoring of hyporheic zone biogeochemistry. UK
883 Environment Agency Science Report SC030155/SR3, 1–44.

884 Brunet, P., Clément, R., & Bouvier, C. (2010). Monitoring soil water content and deficit using Electrical
885 Resistivity Tomography (ERT) - A case study in the Cevennes area, France. Journal of
886 Hydrology, 380(1-2), 146–153. https://doi.org/10.1016/j.jhydrol.2009.10.032

887 Brunke, M., & Gonser, T. (1997). The ecological significance of exchange processes between rivers and
888 groundwater. Freshwater Biology, 37(1), 1–33. https://doi.org/10.1046/j.1365-
889 2427.1997.00143.x

890 Buss, S. R., Cai, Z., Cardenas, B., Fleckenstein, J., Hannah, D. M., Hepell, K., Hulme, P., Ibrahim, T.,
891 Käser, D., Krause, S., Lawler, D.., Lerner, D., Mant, J., Malcolm, I., Old, G., Parkin, G., Pickup,
892 R., Pinay, G., Porter, J., Rhoes, G., Richie, A., Riley, J., Robertson, A., Sear, D., Shields, B.,
893 Smith, J., Tellam, J., Wood, P. (2009). The Hyporheic Handbook: A handbook on the
894 groundwater – surface water interface and hyporheic zone for environment managers
895 integrated catchment science programme. UK Environment Agency Science
896 Report SC050070, 1–264.

897 Butler, K. E., Nadeau, J., Parrott, R., & Daigle, A. (2004). Delineating Recharge to a River Valley Aquifer
898 by Riverine Seismic and EM Methods. Journal of Environmental and Engineering Geophysics,
899 9(2), 95–109. http://library.seg.org/doi/abs/10.4133/JEEG9.2.95

900 Cardenas, M. B., & Markowski, M. S. (2011). Geoelectrical imaging of hyporheic exchange and mixing
901 of river water and groundwater in a large regulated river. Environmental Science and
902 Technology, 45(4), 1407–1411. https://doi.org/10.1021/es103438a

903 Chambers, J. E., Gunn, D. A., Wilkinson, P. B., Meldrum, P. I., Haslam, E., Holyoake, S., Kirkham, M.,
904 Kuras, O., Merrit, A., & Wragg, J. (2014a). 4D electrical resistivity tomography monitoring of
905 soil moisture dynamics in an operational railway embankment. Near Surface Geophysics,
906 12(1), 61–72. https://doi.org/10.3997/1873-0604.2013002

907 Chambers, J. E., Wilkinson, P. B., Uhlemann, S., Sorensen, J. P. R., Roberts, C., Newell, A. J., Ward, W.
908 O. C., Binley, A., Williams, P. J., Goody, D. C., Old, G., & Bai, L. (2014b). Derivation of lowland
909 riparian wetland deposit architecture using geophysical image analysis and interface

detection. Water Resources Research, 50(7), 5886–5905. https://doi.org/10.1002/2012WR013085

Chambers, J. E., Meldrum, P. I., Wilkinson, P. B., Ward, W., Jackson, C., Matthews, B., Joel, P., Kuras, O., Bai, L., Uhlemann, S., & Gunn, D. (2015). Spatial monitoring of groundwater drawdown and rebound associated with quarry dewatering using automated time-lapse electrical resistivity tomography and distribution guided clustering. Engineering Geology, 193, 412–420. https://doi.org/10.1016/j.enggeo.2015.05.015

Chandler, I. D., Guymer, I., Pearson, J. M., & van Egmond, R. (2016). Vertical variation of mixing within porous sediment beds below turbulent flows I. Water Resources Research, 52, 3493–3509. https://doi.org/10.1002/2015WR018274

Chen, J., Hubbard, S. S., & Williams, K. H. (2013). Data-driven approach to identify field-scale biogeochemical transitions using geochemical and geophysical data and hidden Markov models: Development and application at a uranium-contaminated aquifer. Water Resources Research, 49(10), 6412–6424. https://doi.org/10.1002/wrcr.20524

Christensen, N. B., Sørensen, K. I. (1998). Surface and borehole electric and electromagnetic methods for hydrogeological investigations. European Journal of Engineering and Environmental Geophysics 3 (1), 75–90.

Christiansen, A., Pedersen, J., Auken, E., Søe, N., Holst, M., & Kristiansen, S. (2016). Improved Geoarchaeological Mapping with Electromagnetic Induction Instruments from Dedicated Processing and Inversion. Remote Sensing, 8(12), 1022. https://doi.org/10.3390/rs8121022

Christiansen, L., Binning, P. J., Rosbjerg, D., Andersen, O. B., & Bauer-Gottwein, P. (2011). Using time-lapse gravity for groundwater model calibration: An application to alluvial aquifer storage. Water Resources Research, 47(6), W06503, 1-12. https://doi.org/10.1029/2010WR009859

933 Colombero, C., Comina, C., Gianotti, F., & Sambuelli, L. (2014). Waterborne and on-land electrical
934 surveys to suggest the geological evolution of a glacial lake in NW Italy. Journal of Applied
935 Geophysics, 105, 191–202. https://doi.org/10.1016/j.jappgeo.2014.03.020

936 Comas, X., Slater, L., & Reeve, A. (2007). In situ monitoring of free-phase gas accumulation and release
937 in peatlands using ground penetrating radar (GPR). Geophysical Research Letters, 34(6),
938 L06402, 1–5. https://doi.org/10.1029/2006GL029014

939 Comas, X., Kettridge, N., Binley, A., Slater, L., Parsekian, A., Baird, A. J., Strack, M. & Waddington, J. M.
940 (2014). The effect of peat structure on the spatial distribution of biogenic gases within bogs.
941 Hydrological Processes, 28(22), 5483–5494. https://doi.org/10.1002/hyp.10056

942 Constable, S. C. (1987). Occam's inversion: A practical algorithm for generating smooth models from
943 electromagnetic sounding data. Geophysics, 52(3), 289-300.
944 https://doi.org/10.1190/1.1442303

945 Cook, P. G., & Herczeg, A. L. (2000). Environmental Tracers in Subsurface Hydrology. New York, US:
946 Springer. https://link.springer.com/book/10.1007%2F978-1-4615-4557-6

947 Coscia, I., Greenhalgh, S. A., Linde, N., Doetsch, J., Marescot, L., Günther, T., Vogt, T., & Green, A. G.
948 (2011). 3D crosshole ERT for aquifer characterization and monitoring of infiltrating river
949 water. Geophysics, 76(2), G49–G59. https://doi.org/10.1190/1.3553003

950 Coscia, I., Linde, N., Greenhalgh, S., Vogt, T., & Green, A. (2012). Estimating traveltimes and
951 groundwater flow patterns using 3D time-lapse crosshole ERT imaging of electrical resistivity
952 fluctuations induced by infiltrating river water. Geophysics, 77(4), E239-E250.
953 https://doi.org/10.1190/geo2011-0328.1

954 Crook, N., Zarnetske, J., Haggerty, R., Robinson, D. A., Binley, A., Knight, R., Zarnetske, J., & Haggerty,
955 R. (2008). Electrical resistivity imaging of the architecture of substream sediments. Water
956 Resources Research, 44(4), W00D13, 1-11. https://doi.org/10.1029/2008WR006968

957 Daily, W., Ramirez, A., & Binley, A. (2004). Remote Monitoring of Leaks in Storage Tanks using
958 Electrical Resistance Tomography: Application at the Hanford Site. Journal of Environmental
959 and Engineering Geophysics, 9(1), 11-24. http://dx.doi.org/10.4133/JEEG9.1.11

960 Daily, W., Ramirez, A., Binley, A., & LaBrecque, D. (2005). 17. Electrical resistance tomography-theory
961 and practice. In: Butler, D. K. (Editor). Near-Surface Geophysics. Oklahoma, US: Society of
962 Exploration Geophysicists. p525–550. http://dx.doi.org/10.1190/1.9781560801719

963 Day-Lewis, F. D., & Lane, J. W. (2004). Assessing the resolution-dependent utility of tomograms for
964 geostatistics. Geophysical Research Letters, 31(7), L07503, 1–4.
965 https://doi.org/10.1029/2004GL019617

966 Day-Lewis, F. D., White, E. A., Johnson, C. D., Lane, J. W., Belaval, M. (2006). Continuous resistivity
967 profiling to delineate submarine groundwater discharge—examples and limitations. The
968 Leading Edge, 25(6), 724-728. http://library.seg.org/doi/abs/10.1190/1.2210056

969 De Smedt, P., Delefortrie, S., & Wyffels, F. (2016). Identifying and removing micro-drift in ground-
970 based electromagnetic induction data. Journal of Applied Geophysics, 131, 14–22.
971 https://doi.org/10.1016/j.jappgeo.2016.05.004

972 Doetsch, J., Linde, N., Pessognelli, M., Green, A. G., & Günther, T. (2012a). Constraining 3-D electrical
973 resistance tomography with GPR reflection data for improved aquifer characterization.
974 Journal of Applied Geophysics, 78, 68–76. https://doi.org/10.1016/j.jappgeo.2011.04.008

975 Doetsch, J., Linde, N., Vogt, T., Binley, A., & Green, A. G. (2012b). Imaging and quantifying salt-tracer
976 transport in a riparian groundwater system by means of 3D ERT monitoring. Geophysics,
977 77(5), B207-B218. https://doi.org/10.1190/geo2012-0046.1

978 Dorn, C., Linde, N., Borgne, T. Le, Bour, O., & Baron, L. (2011). Single-hole GPR reflection imaging of
979 solute transport in a granitic aquifer. Geophysical Research Letters, 1–11.
980 https://doi.org/10.1029/2011GL047152.1

981 Doro, K. O., Leven, C., & Cirpka, O. A. (2013). Delineating subsurface heterogeneity at a loop of River
982 Steinlach using geophysical and hydrogeological methods. Environmental Earth Sciences, 69,
983 335–348. https://doi.org/10.1007/s12665-013-2316-0

984 Dudley-Southern, M., & Binley, A. (2015). Temporal responses of groundwater-surface water
985 exchange to successive storm events. Water Resources Research, 51(2), 1112–1126.
986 https://doi.org/10.1002/2014WR016259

987 Elliott, H., & Brooks, N. H. (1997). Transfer of nonsorbing solutes to a streambed with bed forms:
988 Theory. Water Resources Research 33(1), 123–136.

989 Elwaseif, M., Robinson, J., Day-Lewis, F. D., Ntarlagiannis, D., Slater, L. D., Lane Jr., J. W., Minsley, B. J.
990 Schultz, G. (2017). A matlab-based frequency-domain electromagnetic inversion code
991 (FEMIC) with graphical user interface. Computers and Geosciences, 99, 61–71.
992 https://doi.org/10.1016/j.cageo.2016.08.016

993 EMTOMO. (2013). EM4Soil: Software for Electromagnetic Tomography. http://www.emtomo.com/

994 Everett, M. E., & Meju, M. A. (2005). Electromagnetic induction. In: Rubin, Y. & Hubbard, S. S.
995 (Editors). Hydrogeophysics, Vol. 2. Netherlands: Springer. p157–183.
996 https://doi.org/10.1080/00107516108202659

997 Findlay, S., Strayer, D., Goumbala, C., & Gould, K. (1993). Metabolism of streamwater dissolved
998 organic carbon in the shallow hyporheic zone. Limnology and Oceanography, 38(7), 1493–
999 1499. https://doi.org/10.4319/lo.1993.38.7.1493

1000 Findlay, S. (1995). Importance of surface-subsurface exchange in stream ecosystems: The hyporheic
1001 zone. Limnology and Oceanography, 40(1), 159–164.
1002 https://doi.org/10.4319/lo.1995.40.1.0159

1003 Fitterman, D. V. (2015). Tools and Techniques: Active-Source Electromagnetic Methods. In: Schubert,
1004 G. (Editor). Treatise on Geophysics, 2nd Edition, Vol. 11. Oxford, UK: Elsevier. p233-259.
1005 https://doi.org/10.1016/B978-0-444-53802-4.00193-7

1006 Fleckenstein, J. H., Krause, S., Hannah, D. M., & Boano, F. (2010). Groundwater-surface water
1007 interactions: New methods and models to improve understanding of processes and
1008 dynamics. Advances in Water Resources, 33(11), 1291–1295.
1009 https://doi.org/10.1016/j.advwatres.2010.09.011

1010 Flores Orozco, A., Williams, K. H., Long, P. E., Hubbard, S. S., & Kemna, A. (2011). Using complex
1011 resistivity imaging to infer biogeochemical processes associated with bioremediation of an
1012 uranium-contaminated aquifer. Journal of Geophysical Research: Biogeosciences, 116(3), 1–
1013 17. https://doi.org/10.1029/2010JG001591

1014 Freeze, R. A., & Witherspoon, P. A. (1967). Theoretical Analysis Regional Groundwater Flow: 2. Effect
1015 of Water-Table Configuration and Subsurface Permeability Variation. Water Resources
1016 Research, 3(2), 623–634. http://onlinelibrary.wiley.com/doi/10.1029/WR003i002p00623

1017 Froese, D. G., Smith, D. G., & Clement, D. T. (2005). Characterizing large river history with shallow
1018 geophysics: Middle Yukon River, Yukon Territory and Alaska. Geomorphology, 67(3–4), 391–
1019 406. https://doi.org/10.1016/j.geomorph.2004.11.011

1020 Gallardo, L. A., & Meju, M. A. (2004). Joint two-dimensional DC resistivity and seismic travel time
1021 inversion with cross-gradients constraints. Journal of Geophysical Research, 109, 1–11.
1022 https://doi.org/10.1029/2003JB002716

1023 Gandy, C. J., Smith, J. W. N., & Jarvis, A. P. (2007). Attenuation of mining-derived pollutants in the
1024 hyporheic zone: A review. Science of the Total Environment, 373(2–3), 435–446.
1025 https://doi.org/10.1016/j.scitotenv.2006.11.004

1026 Garré, S., Javaux, M., Vanderborght, J., Pagès, L., Vereecken, H. (2011) Three-Dimensional electrical
1027 resistivity tomography to monitor root zone water dynamics. Vadose Zone Journal, 10(1),
1028 412–424.

1029 Gilliam, J. W. (1994). Riparian wetlands and water quality. Journal of Environmental Quality. 23(5),
1030 896-900.

1031 Glover, P. W. J. (2015). Geophysical Properties of the Near Surface Earth: Electrical Properties. In:
1032 Schubert, G. (Editor). Treatise on Geophysics, 2nd Edition, Vol. 11. Oxford, UK: Elsevier. p89–
1033 137. https://doi.org/10.1016/B978-0-444-53802-4.00190-1

1034 Gomez-Velez, J. D., & Harvey, J. W. (2014). A hydrogeomorphic river network model predicts where
1035 and why hyporheic exchange is important in large basins. Geophysical Research Letters,
1036 41(18), 6403–6412. https://doi.org/10.1002/2014GL061099

1037 González-Pinzón, R., Ward, A. S., Hatch, C. E., Wlostowski, A. N., Singha, K., Gooseff, M. N., Haggerty,
1038 R., Harvey, J. W., Cirpka, O. A., & Brock, J. T. (2015). A field comparison of multiple
1039 techniques to quantify groundwater – surface-water interactions. Freshwater Science, 34(1),
1040 139–160. https://doi.org/10.1086/679738

1041 Gooseff, M. N. (2010). Defining hyporheic zones- Advancing our conceptual and operational
1042 definitions of where stream water and groundwater meet. Geography Compass, 4(8), 945-
1043 955.

1044 Greswell, R. B. (2005). High-resolution in situ monitoring of flow between aquifers and surface waters.
1045 UK Environment Agency Science Report SC030155/SR4, 1–44.

1046 Günther, T. & Rucker, C. (2006). A new joint inversion approach applied to the combined tomography
1047 of DC resistivity and refraction data. Proceedings of the 19th EEGS Annual Meeting, Seattle,
1048 USA.

1049 Hare, D. K., Briggs, M. A., Rosenberry, D. O., Boutt, D. F., & Lane, J. W. (2015). A comparison of thermal
1050 infrared to fiber-optic distributed temperature sensing for evaluation of groundwater
1051 discharge to surface water. Journal of Hydrology, 530, 153–166.
1052 https://doi.org/10.1016/j.jhydrol.2015.09.059

1053 Harrington, G. A., Payton Gardner, W., & Munday, T. J. (2014). Tracking Groundwater Discharge to a
1054 Large River using Tracers and Geophysics. Ground Water, 52(6), 837–852.
1055 https://doi.org/10.1111/gwat.12124

1056 Harvey, J. W., Germann, P. F., & Odum, W. E. (1987). Geomorphological Control of Subsurface
1057 Hydrology in the Creekbank Zone of Tidal Marshes. Estuarine, Coastal and Shelf Science, 25,
1058 677–691.

1059 Harvey, J. W., Wagner, B. J., & Bencala, K. E. (1996). Evaluating the reliability of stream tracer
1060 approach to characterize stream-subsurface water exchange. Water Resources Research,
1061 32(8), 2441–2451. http://onlinelibrary.wiley.com/doi/10.1029/96WR01268

1062 Harvey, J. W., & Fuller, C. C. (1998). Effect of enhanced manganese oxidation in the hyporheic zone on
1063 basin-scale geochemical mass balance. Water Resources Research, 34(4), 623–636.
1064 https://doi.org/10.1029/97WR03606

1065 Harvey, J. W., Drummond, J. D., Martin, R. L., McPhillips, L. E., Packman, A. I., Jerolmack, D. J.,
1066 Stonedahl, S. H., Aubeneau, A. F., Sawyer, A. H., Larsen, L. H., & Tobias, C. R. (2012).
1067 Hydrogeomorphology of the hyporheic zone : Stream solute and fine particle interactions
1068 with a dynamic streambed. Journal of Geophysical Research, 117(G00N11), 1–20.
1069 https://doi.org/10.1029/2012JG002043

1070 Harvey, J. W., & Gooseff, M. N. (2015). River corridor science: Hydrologic exchange and ecological
1071 consequences from bedforms to basins. Water Resources Research, 51(9), 6893–6922.
1072 https://doi.org/10.1002/2015WR017617

1073 Hayashi, M., & Rosenberry, D. O. (2002). Effects of Ground Water Exchange on the Hydrology and
1074 Ecology of Surface Water. Ground Water, 40(3), 309-316.

1075 He, X., Koch, J., Sonnenborg, T. O., Jorgensen, F., Schamper, C., & Refsgaard, J. C. (2014). Transition
1076 probability-based stochastic geological modeling using airborne geophysical data and
1077 borehole data. Water Resources Research, 50(4), 3147–3169.
1078 https://doi.org/10.1002/2013WR014593

1079 Henderson, R. D., Day-Lewis, F. D., Abarca, E., Harvey, C. F., Karam, H. N., Liu, L., & Lane, J. W. J.
1080 (2010). Marine electrical resistivity imaging of submarine groundwater discharge: sensitivity
1081 analysis and application in Waquoit Bay, Massachusetts, USA. Hydrogeology Journal, 18,
1082 173–185. https://doi.org/10.1007/s10040-009-0498-z

1083 Heppell, C., Louise Heathwaite, A., Binley, A., Byrne, P., Ullah, S., Lansdown, K., Keenan, P., Trimmer,
1084 M., & Zhang, H. (2014). Interpreting spatial patterns in redox and coupled water-nitrogen

fluxes in the streambed of a gaining river reach. Biogeochemistry, 117(2), 491–509. https://doi.org/10.1007/s10533-013-9895-4

Herckenrath, D., Fiandaca, G., Auken, E., & Bauer-Gottwein, P. (2013). Sequential and joint hydrogeophysical inversion using a field-scale groundwater model with ERT and TDEM data. Hydrology and Earth System Sciences, 17(10), 4043–4060. https://doi.org/10.5194/hess-17-4043-2013

Hering, D., Borja, A., Carstensen, J., Carvalho, L., Elliott, M., Feld, C. K., Heiskanen, A. S., Johnson, R. K., Moe, J., Pont, D., Solheim, A. L., van de Bund, W. (2010). The European Water Framework Directive at the age of 10: A critical review of the achievements with recommendations for the future. Science of the Total Environment, 408(19), 4007–4019. https://doi.org/10.1016/j.scitotenv.2010.05.031

Hester, E. T., Cardenas, M. B., Haggerty, R., & Apte, S. V. (2017). The importance and challenge of hyporheic mixing. Water Resources Research, 53, 3565–3575. https://doi.org/10.1002/2016WR020005

Hester, E. T., Young, K. I., & Widdowson, M. A. (2013). Mixing of surface and groundwater induced by riverbed dunes: Implications for hyporheic zone definitions and pollutant reactions. Water Resources Research, 49(9), 5221–5237. https://doi.org/10.1002/wrcr.20399

Hinnell, A. C., Ferré, T. P. A., Vrugt, J. A., Huisman, J. A., Moysey, S., Rings, J., & Kowalsky, M. B. (2010). Improved extraction of hydrologic information from geophysical data through coupled hydrogeophysical inversion. Water Resources Research, 46(4), W00D40, 1-14. https://doi.org/10.1029/2008WR007060

Holliger, K. (2008). Groundwater Geophysics: From Structure and Porosity Towards Permeability? In: Darnault, C. J. G. (Editor). Overexploitation and Contamination of Shared Groundwater

1108 Resources: Management, (Bio)Technological, and Political Approaches to Avoid Conflicts.
1109 Dordrecht, Netherlands: Springer. p49-65 https://doi.org/10.1007/978-1-4020-6985-7_4

1110 Hoversten, G. M., Cassassuce, F., Gasperikova, E., Newman, G. A., Chen, J., Rubin, Y., Hou, Z. & Vasco,
1111 D. (2006). Direct reservoir parameter estimation using joint inversion of marine seismic AVA
1112 and CSEM data. Geophysics, 71(3), C1–C13.

1113 Huang, J., Scudiero, E., Clary, W., Corwin, D. L., & Triantafilis, J. (2017). Time-lapse monitoring of soil
1114 water content using electromagnetic conductivity imaging. Soil Use and Management, 33,
1115 191–204. https://doi.org/10.1111/sum.12261

1116 Hubbard, S. S., & Linde, N. (2011). Hydrogeophysics. In: Wilderer, P. (Editor). Treatise on Water
1117 Science, Vol. 2. Oxford, UK: Academic Press. p401–432

1118 Huisman, J. A., Hubbard, S. S., Redman, J. D., & Annan, A. P. (2003). Measuring Soil Water Content
1119 with Ground Penetrating Radar: A Review. Vadose Zone Journal, 2, 476–491.

1120 Huisman, J. A., Rings, J., Vrugt, J. A., Sorg, J., & Vereecken, H. (2010). Hydraulic properties of a model
1121 dike from coupled Bayesian and multi-criteria hydrogeophysical inversion. Journal of
1122 Hydrology, 380(1–2), 62–73. https://doi.org/10.1016/j.jhydrol.2009.10.023

1123 Ingham, M., McConchie, J. A., Wilson, S. R., & Cozens, N. (2006). Measuring and monitoring saltwater
1124 intrusion in shallow unconfined coastal aquifers using direct current resistivity traverses.
1125 Journal of Hydrology New Zealand, 45(2), 69–82.

1126 Irvine, D. J., & Lautz, L. K. (2015). High resolution mapping of hyporheic fluxes using streambed
1127 temperatures: Recommendations and limitations. Journal of Hydrology, 524, 137–146.
1128 https://doi.org/10.1016/j.jhydrol.2015.02.030

1129 Irvine, D. J., Cartwright, I., Post, V. E. A., Simmons, C. T., & Banks, E. W. (2016). Uncertainties in vertical
1130 groundwater fluxes from 1-D steady state heat transport analyses caused by heterogeneity,

multidimensional flow, and climate change. Water Resources Research, 52, 813–826. https://doi.org/10.1002/2015WR017702

Jackson, M. D. (2015). Tools and Techniques: Self-Potential Methods. In: Schubert, G. (Editor). Treatise on Geophysics, 2nd Edition, Vol. 11. Oxford, UK: Elsevier. p261–293 https://doi.org/10.1016/B978-0-444-53802-4.00208-6

Jacob, R. W., & Hermance, J. F. (2004). Precision GPR measurements: assessing and compensating for instrument drift. Proceedings of the Tenth International Conference on Grounds Penetrating Radar, Delft, Netherlands, 159–162.

JafarGandomi, A., & Binley, A. (2013). A Bayesian trans-dimensional approach for the fusion of multiple geophysical datasets. Journal of Applied Geophysics, 96, 38–54. https://doi.org/10.1016/j.jappgeo.2013.06.004

Jardani, A., Revil, A., & Dupont, J. P. (2013). Advances in Water Resources Stochastic joint inversion of hydrogeophysical data for salt tracer test monitoring and hydraulic conductivity imaging. Advances in Water Resources, 52, 62–77. https://doi.org/10.1016/j.advwatres.2012.08.005

Johnson, T. C., Versteeg, R. J., Hauang, H. & Routh, P. S. (2009). Data-domain correlation approach for joint hydrogeologic inversion of time-lapse hydrogeologic and geophysical data. Geophysics, 74(6). F127–F140. http://library.seg.org/doi/abs/10.1190/1.3237087

Johnson, T. C., Versteeg, R. J., Ward, A., Day-Lewis F. D., & Revil, A. (2010). Improved hydrogeophysical characterization and monitoring through parallel modeling and inversion of time-domain resistivity and induced-polarization data. Geophysics, 75(4), WA27–WA41

Johnson, T. C., Slater, L. D., Ntarlagiannis, D., Day-Lewis, F. D., & Elwaseif, M. (2012). Monitoring groundwater-surface water interaction using time-series and time-frequency analysis of

transient three-dimensional electrical resistivity changes. Water Resources Research, 48(7), W07506, 1-12. https://doi.org/10.1029/2012WR011893

Johnson, T. C., Rucker, D. F., & Glaser, D. R. (2015). Near-Surface Geophysics at the Hanford Nuclear Site, the United States. In: Schubert, G. (Editor). Treatise on Geophysics, 2nd Edition, Vol. 11. Oxford, UK: Elsevier. p571–595. https://doi.org/10.1016/B978-0-444-53802-4.00205-0

Jørgensen, F., Scheer, W., Thomsen, S., Sonnenborg, T. O., Hinsby, K., Wiederhold, H., Schamper, C., Burschil, T., Roth, B., Kirsch, R., & Auken, E. (2012). Transboundary geophysical mapping of geological elements and salinity distribution critical for the assessment of future sea water intrusion in response to sea level rise. Hydrology and Earth System Sciences, 16(7), 1845–1862. https://doi.org/10.5194/hess-16-1845-2012

Kaika, M. (2003). The Water Framework Directive: A new directive for a changing social, political and economic European framework. European Planning Studies, 11(3), 299–316. https://doi.org/10.1080/0965431032000070802

Kalbus, E., Reinstorf, F., & Schirmer, M. (2006). Measuring methods for groundwater, surface water and their interactions: A review. Hydrology and Earth System Sciences Discussions, 3(4), 873–887. https://doi.org/10.5194/hessd-3-1809-2006

Käser, D. H., Binley, A., Heathwaite, A. L., & Krause, S. (2009). Spatio-temporal variations of hyporheic flow in a riffle-step-pool sequence. Hydrological Processes, 23(15), 2138–2149. https://doi.org/10.1002/hyp

Käser, D., Binley, A. M., & Louise Heathwaite, A. (2013). On the importance of considering channel microforms in groundwater models of hyporheic exchange. River Research and Applications, 29(4), 528–535. https://doi.org/10.1002/rra

1175 Kelly, B. F. J., Allen, D., Ye, K., & Dahlin, T. (2009). Continuous electrical imaging for mapping aquifer
1176 recharge along reaches of the Namoi River in Australia. Near Surface Geophysics, 7(4), 259–
1177 270.

1178 Kelly, S. E., & Murdoch, L. C. (2003). Measuring the Hydraulic Conductivity of Shallow Submerged
1179 Sediments. Ground Water, 41(4), 431–439.

1180 Kemna, A., Binley, A., & Slater, L. (2004). Crosshole IP imaging for engineering and environmental
1181 applications, Geophysics. 69(1), 97–107.

1182 Kemna, A., Binley, A., Cassiani, G., Niederleithinger, E., Revil, A., Slater, L., Williams, K., Flores Orozco,
1183 A., Haegel, H., Kruschwitz, S., Leroux, V. & Zimmermann, E. (2012). An overview of the
1184 spectral induced polarization method for near-surface applications. Near Surface
1185 Geophysics, 10, 453–468. https://doi.org/10.3997/1873-0604.2012027

1186 Kemna, A., Binley, A., Ramirez, A., & Daily, W. (2000). Complex resistivity tomography for
1187 environmental applications. Chemical Engineering Journal, 77(1), 11–18.

1188 Kennedy, C. D., Genereux, D. P., Corbett, D. R., & Mitasova, H. (2009). Relationships among
1189 groundwater age, denitrification, and the coupled groundwater and nitrogen fluxes through
1190 a streambed. Water Resources Research, 45(9), W09402, 1–15.
1191 https://doi.org/10.1029/2008WR007400

1192 Kiel, B. A., & Cardenas, B. M. (2014). Lateral hyporheic exchange throughout the Mississippi River
1193 network. Nature Geoscience, 7, 413–417. https://doi.org/10.1038/ngeo2157

1194 King, J. N., Mehta, A. J., & Dean, R. G. (2009). Generalized analytical model for benthic water flux
1195 forced by surface gravity waves. Journal of Geophysical Research, 114(4), C04004, 1–14.
1196 https://doi.org/10.1029/2008JC005116

1197 Kinnear, J. A., Binley, A., Duque, C., & Engesgaard, P. K. (2013). Using geophysics to map areas of
1198 potential groundwater discharge into Ringkøbing Fjord, Denmark. The Leading Edge. 32(7),
1199 792-796.

1200 Kirkegaard, C., Sonnenborg, T. O., Auken, E., & Jørgensen, F. (2011). Salinity Distribution in
1201 Heterogeneous Coastal Aquifers Mapped by Airborne Electromagnetics. Vadose Zone
1202 Journal, 10(1), 125–135. https://doi.org/10.2136/vzj2010.0038

1203 Kowalsky, M. B., Finsterle, S., Peterson, J., Hubbard, S., Rubin, Y., Majer, E., Ward, A., & Gee, G. (2005).
1204 Estimation of field-scale soil hydraulic and dielectric parameters through joint inversion of
1205 GPR and hydrological data. Water Resources Research, 41(11), 1–19.
1206 https://doi.org/10.1029/2005WR004237

1207 Kruse, S. (2013). Near-Surface Geophysics in Geomorphology. In: Shroder, J. & Bishop, M. P. (Editors).
1208 Treatise on Geomorphology, Remote Sensing and GIScience in Geomorphology, Vol. 3.
1209 California, US: Academic Press. p103–129. https://doi.org/10.1016/B978-0-12-374739-
1210 6.00047-6

1211 Kuras, O., Pritchard, J. D., Meldrum, P. I., Chambers, J. E., Wilkinson, P. B., Ogilvy, R. D., & Wealthall, G.
1212 P. (2009). Monitoring hydraulic processes with automated time-lapse electrical resistivity
1213 tomography (ALERT). Comptes Rendus Geoscience, 341(10–11), 868–885.
1214 https://doi.org/10.1016/j.crte.2009.07.010

1215 Lambot, S., Antoine, M., van den Bosch, I., Slob, E. C., & Vanclooster, M. (2004). Electromagnetic
1216 Inversion of GPR Signals and Subsequent Hydrodynamic Inversion to Estimate Effective
1217 Vadose Zone Hydraulic Properties. Vadose Zone Journal, 3(4), 1072–1081.
1218 https://doi.org/10.2136/vzj2004.1072

Lambot, S., Slob, E. C., Vanclooster, M., & Vereecken, H. (2006). Closed loop GPR data inversion for soil hydraulic and electric property determination. Geophysical Research Letters, 33(21), L21405, 4–5. https://doi.org/10.1029/2006GL027906

Lansdown, K., Heppell, C. M., Trimmer, M., Binley, A., Heathwaite, A. L., Byrne, P., & Zhang, H. (2015). The interplay between transport and reaction rates as controls on nitrate attenuation in permeable, streambed sediments. Journal of Geophysical Research: Biogeosciences, 120(6), 1093–1109. https://doi.org/10.1002/2014JG002874

Larsen, L. G., Harvey, J. W., & Maglio, M. M. (2014). Dynamic hyporheic exchange at intermediate timescales: Testing the relative importance of evapotranspiration and flood pulses Minutes Hours Days Weeks Months Years Decades. Water Resources Research, 50, 318–335. https://doi.org/10.1002/2013WR014195

Lautz, L. K., & Siegel, D. I. (2006). Modeling surface and ground water mixing in the hyporheic zone using MODFLOW and MT3D. Advances in Water Resources, 29(11), 1618–1633. https://doi.org/10.1016/j.advwatres.2005.12.003

Lavoué, F., Van Der Kruk, J., Rings, J., André, F., Moghadas, D., Huisman, J.A., Lambot, S., Weihermüller, L., Vanderborght, J., Vereecken, H., (2010). Electromagnetic induction calibration using apparent electrical conductivity modelling based on electrical resistivity tomography. Near Surface Geophysics, 8(6), 553–561.

Leroy, P., & Revil, A. (2009). Spectral induced polarization of clays and clay-rocks. Journal of Geophysical Research, 11(B10202), 1–21.

Lesmes, D. P., & Frye, K. M. (2001). Influence of pore fluid chemistry on the complex conductivity and induced polarization responses of Berea sandstone. Journal of Geophysical research: Solid Earth, 106(B3), 4079–4090.

1242 Lin, H. (2010). Earth's Critical Zone and hydropedology: concepts, characteristics, and advances.
1243 Hydrology and Earth System Sciences, 14, 25–45.

1244 Linde, N., Binley, A., Tryggvason, A., Pedersen, L. B., & Revil, A. (2006). Improved hydrogeophysical
1245 characterization using joint inversion of cross-hole electrical resistance and ground-
1246 penetrating radar traveltime data. Water Resources Research, 42(12), W12404, 1–16.
1247 https://doi.org/10.1029/2006WR005131

1248 Linde, N., & Revil, A. (2007). Inverting self-potential data for redox potentials of contaminant plumes.
1249 Geophysical Research Letters, 34(14), L14302, 1–5. https://doi.org/10.1029/2007GL030084

1250 Linde, N., Renard, P., Mukerji, T., & Caers, J. (2015). Geological realism in hydrogeological and
1251 geophysical inverse modeling: A review. Water Resources Research 86, 86–90.

1252 Loheide, S. P., & Lundquist, J. D. (2009). Snowmelt-induced diel fluxes through the hyporheic zone.
1253 Water Resources Research, 45(1), 1–9. https://doi.org/10.1029/2008WR007329

1254 Loke, M. H., Chambers, J. E., Rucker, D. F., Kuras, O., & Wilkinson, P. B. (2013). Recent developments
1255 in the direct-current geoelectrical imaging method. Journal of Applied Geophysics, 95, 135–
1256 156. https://doi.org/10.1016/j.jappgeo.2013.02.017

1257 Loke, M. H., Wilkinson, P. B., Chambers, J. E., Uhlemann, S. S., & Sorensen, J. P. R. (2015). Optimized
1258 arrays for 2-D resistivity survey lines with a large number of electrodes. Journal of Applied
1259 Geophysics, 112, 136–146. https://doi.org/10.1016/j.jappgeo.2014.11.011

1260 Malard, F., Tockner, K., Dole-Olivier, M., & Ward, J. V. (2002). A landscape perspective of surface –
1261 subsurface hydrological exchanges in river corridors. Freshwater Biology, 47(4), 621–640.
1262 https://doi.org/10.1046/j.1365-2427.2002.00906.x

1263 Malzone, J. M., Anseeuw, S. K., Lowry, C. S., & Allen-King, R. (2016). Temporal Hyporheic Zone
1264 Response to Water Table Fluctuations. Groundwater, 54(2), 274–285.
1265 https://doi.org/10.1111/gwat.12352

1266 Mansoor, N., Slater, L., Artigas, F., & Auken, E. (2006). High-resolution geophysical characterization of
1267 shallow-water wetlands. Geophysics, 71(4), B101–B109. https://doi.org/10.1190/1.2210307

1268 Mansoor, N., & Slater, L. (2007). Aquatic electrical resistivity imaging of shallow-water wetlands.
1269 Geophysics, 72(5), F211–F221. https://doi.org/10.1190/1.2750667

1270 Marzadri, A., Tonina, D., & Bellin, A. (2013a). Effects of stream morphodynamics on hyporheic zone
1271 thermal regime. Water Resources Research, 49, 2287–2302.
1272 https://doi.org/10.1002/wrcr.20199

1273 Marzadri, A., Tonina, D., & Bellin, A. (2013b). Quantifying the importance of daily stream water
1274 temperature fluctuations on the hyporheic thermal regime: Implication for dissolved oxygen
1275 dynamics. Journal of Hydrology, 507, 241–248.
1276 https://doi.org/10.1016/j.jhydrol.2013.10.030

1277 Marzadri, A., Dee, M. M., Tonina, D., Bellin, A., & Tank, J. L. (2017). Role of surface and subsurface
1278 processes in scaling N2O emissions along riverine networks. Proceedings of the National
1279 Academy of Sciences, 114(17), 4330–4335.

1280 Meier, P., Kalscheuer, T., Podgorski, J. E., Kgotlhang, L., Green, A. G., Greenhalgh, S., Rabenstein, L.,
1281 Doetsch, J., Kinzelbach, W., Auken, Esben, Mikkelsen, P., Foged, N., Jaba, B. C., Tshoso, G.,
1282 Ntibinyane, O. (2014). Hydrogeophysical investigations in the western and north-central
1283 Okavango Delta (Botswana) based on helicopter and ground-based transient
1284 electromagnetic data and electrical resistance tomography. Geophysics, 79(5), B201–B211.
1285 https://doi.org/10.1190/geo2014-0001.1

1286 Menichino, G. T., Ward, A. S., & Hester, E. T. (2014). Macropores as preferential flow paths in meander
1287 bends. Hydrological Processes, 28(3), 482–495. https://doi.org/10.1002/hyp.9573

1288 Menichino, G. T., & Hester, E. T. (2014). Hydraulic and thermal effects of in-stream structure-induced
1289 hyporheic exchange across a range of hydraulic conductivities. Water Resources Research,
1290 50, 4643–4661. https://doi.org/10.1002/2013WR014758

1291 Menke W. (2012). Geophysical Data Analysis: Discrete Inverse Theory, 3rd Edition. Massachusetts, US:
1292 Elsevier.

1293 Mermillod-Blondin, F., Winiarski, T., Foulquier, A., Perrissin, A., & Marmonier, P. (2015). Links between
1294 sediment structures and ecological processes in the hyporheic zone: ground-penetrating
1295 radar as a non-invasive tool to detect subsurface biologically active zones. Ecohydrology,
1296 8(4), 626–641. https://doi.org/10.1002/eco.1530

1297 Michot, D., Benderitter, Y., Doringny, A., Nicoullaud, B., King, D., & Tabbagh, A. (2003). Spatial and
1298 temporal monitoring of soil water content with an irrigated corn crop cover using surface
1299 electrical resistivity tomography. Water Resources Research, 39(5), 1–20.
1300 https://doi.org/10.1029/2002WR001581

1301 Miled, M. B. H., & Miller, E. L. (2007). A projection-based level-set approach to enhance conductivity
1302 anomaly reconstruction in electrical resistance tomography. Inverse Problems, 23(6), 2375–
1303 2400. https://doi.org/10.1088/0266-5611/23/6/007

1304 Miller, R. B., Heeren, D. M., Fox, G. A., Halihan, T., Storm, D. E., & Mittelstet, A. R. (2014). The
1305 hydraulic conductivity structure of gravel-dominated vadose zones within alluvial
1306 floodplains. Journal of Hydrology, 513, 229–240.
1307 https://doi.org/10.1016/j.jhydrol.2014.03.046

1308 Minsley, B. (2007). Modelling and inversion of self-potential data. PhD Dissertation. Department of
1309 Earth, Atmospheric, and Planetary Sciences, Massachusetts Institute of Technology.
1310 http://hdl.handle.net/1721.1/40863

1311 Minsley, B. J., Abraham, J. D., Smith, B. D., Cannia, J. C., Voss, C. I., Jorgenson, M. T., Walvoord, M. A.,
1312 Wylie, B. K., Anderson, L., Ball, L. B., Deszcz-Pan, M., Wellman, T. P., & Ager, T. A. (2012).
1313 Airborne electromagnetic imaging of discontinuous permafrost. Geophysical Research
1314 Letters, 39(2), L02503, 1–8. https://doi.org/10.1029/2011GL050079

1315 Mitsch, W. J. (1992). Landscape design and the role of created, restored, and natural riparian wetlands
1316 in controlling nonpoint source pollution. Ecological Engineering, 1(1–2), 27–47.
1317 https://doi.org/10.1016/0925-8574(92)90024-V

1318 Montaron, B. (2009). Connectivity Theory – A New Approach to Modeling Non- Archie Rocks.
1319 Petrophysics, 50(2), 102–115.

1320 Moysey, S., Singha, K., & Knight, R. (2005). A framework for inferring field-scale rock physics
1321 relationships through numerical simulation. Geophysical Research Letters, 32(8), 1–4.
1322 https://doi.org/10.1029/2004GL022152

1323 Musgrave, D. L., and W. S. Reeburgh (1982), Density-driven interstitial water motion in sediments,
1324 Nature, 299(5881), 331–334.

1325 Mwakanyamale, K., Slater, L., Binley, A., & Ntarlagiannis, D. (2012). Lithologic imaging using complex
1326 conductivity: Lessons learned from the Hanford 300 Area. Geophysics, 77(6), E397.
1327 https://doi.org/10.1190/geo2011-0407.1

1328 Nabighian, M.N., and Macnae, J.C. (1991). Time-domain electromagnetic prospecting methods. In
1329 Nabighian, M.N. (Editor). Electromagnetic Methods in Applied Geophysics Theory, Vol. 2.
1330 Oklahoma, US: Society of Exploration Geophysicists. p427–520

1331 Nagorski, S. A., & Moore, J. N. (1999). Arsenic mobilization in the hyporheic zone of a stream. Water
1332 Resources Research, 35(11), 3441–3450. https://doi.org/10.1029/1999WR900204

1333 Naudet, V., Revil, A., Bottero, J. & Bégassat, P. (2003). Relationship between self-potential (SP) signals
1334 and redox conditions in contaminated groundwater. Geophysical Research Letters, 30(21),
1335 1–4. https://doi.org/10.1029/2003GL018096

1336 Naudet, V., Revil, A., Rizzo, E., Bottero, J., & Bégassat, P. (2004). Groundwater redox conditions and
1337 conductivity in a contaminant plume from geoelectrical investigations. Hydrology and Earth
1338 System Sciences, 8(1), 8–22.

1339 Nenna, V., & Knight, R. (2013). Demonstration of a value of information metric to assess the use of
1340 geophysical data for a groundwater application. Geophysics, 79(1), E51–E60.
1341 https://doi.org/10.1190/geo2012-0474.1

1342 Newbold, J. D., O'Neill, R. V, Elwood, J. W., & Van Winkle, W. (1982). Nutrient Spiralling in Streams:
1343 Implications for Nutrient Limitation and Invertebrate Activity. American Naturalist, 120(5),
1344 628–652.

1345 Newell, A. J., Sorensen, J. P. R., Chambers, J. E., Wilkinson., P. B., Uhlemann, S. S., Roberts, C., Gooddy,
1346 D. C., Vane, C. H., & Binley, A. (2015). Fluvial response to late Pleistocene and Holocene
1347 environmental change in a Thames chalkland headwater: the Lambourn of southern
1348 England. Proceedings of the Geologists' Association, 126(6), 683–697.
1349 https://doi.org/10.1016/j.pgeola.2015.08.008

1350 Nyquist, J. E., Freyer, P., & Toran, L. (2008). Stream bottom resistivity tomography to map ground
1351 water discharge. Ground Water, 46(4), 561–569. https://doi.org/10.1111/j.1745-
1352 6584.2008.00432.x

1353 Ogilvy, R. D., Kuras, O., Meldrum, P. I., Wilkinson, P. B., Chambers, J. E, Sen, M., Gisbert, J., Jorreto, S.,
1354 Frances, I., Pulido-Bosch, A., Tsourlos, P. (2009). Automated time-Lapse Electrical Resistivity
1355 Tomography (ALERT) for monitoring Coastal Aquifers. Near Surface Geophysics, 7(5-6), 367–
1356 375.

1357 Oldenborger, G. A., Logan, C. E., Hinton, M. J., Pugin, A. J. M., Sapia, V., Sharpe, D. R., & Russell, H. A. J.
1358 (2016). Bedrock mapping of buried valley networks using seismic reflection and airborne
1359 electromagnetic data. Journal of Applied Geophysics, 128, 191–201.
1360 https://doi.org/10.1016/j.jappgeo.2016.03.006

1361 Oldenburg, D. W., & Li, Y. (1999). Estimating depth of investigation in dc resistivity and IP surveys.
1362 Geophysics, 64(2), 403. https://doi.org/10.1190/1.1444545

1363 Packman, A. I., & MacKay, J. S. (2003). Interplay of stream-subsurface exchange, clay particle
1364 deposition, and streambed evolution. Water Resources Research, 39(4), 1–10.
1365 https://doi.org/10.1029/2002WR001432

1366 Paine, J. G. (2003). Determining salinization extent, identifying salinity sources, and estimating
1367 chloride mass using surface, borehole, and airborne electromagnetic induction methods.
1368 Water Resources Research, 39(3), 1059. https://doi.org/10.1029/2001WR000710

1369 Parsekian, A. D., Comas, X., Slater, L., & Glaser, P. H. (2011). Geophysical evidence for the lateral
1370 distribution of free phase gas at the peat basin scale in a large northern peatland. Journal of
1371 Geophysical Research: Biogeosciences, 116, G03008, 1–14.
1372 https://doi.org/10.1029/2010JG001543

1373 Parsekian, A. D., Singha, K., Minsley, B. J., Holbrook, W. S., & Slater, L. (2015). Multiscale geophysical
1374 imaging of the critical zone. Reviews of Geophysics, 53, 1–26.
1375 https://doi.org/10.1029/88EO01108

Pastick, N. J., Jorgenson, M. T., Wylie, B. K., Minsley, B. J., Ji, L., Walvoord, M. A., Smith, B. D., Abraham, J. D., & Rose, J. R. (2013). Extending airborne electromagnetic surveys for regional active layer and permafrost mapping with remote sensing and ancillary data, Yukon Flats Ecoregion, Central Alaska. Permafrost and Periglacial Processes, 24(3), 184–199.

Phelps, G., Ippolito, C., Lee, R., Spritzer, J., & Yeh, Y. (2014). Investigations into Near-real-time surveying for Geophysical Data Collection using an Autonomous Ground Vehicle. US Geological Survey Open File Report 2014-1013, 1–12.

Pidlisecky, A., Singha, K., & Day-Lewis, F. D. (2011). A distribution-based parametrization for improved tomographic imaging of solute plumes, Geophysical Journal International, 187(1), 214–224. https://doi.org/10.1111/j.1365-246X.2011.05131.x

Power, G., Brown, R. S., & Imhof, J. G. (1999). Groundwater and fish–insights from northern North America. Hydrological Processes, 13(3), 401–422.

Prendergast, L. J., & Gavin, K. (2014). A review of bridge scour monitoring techniques. Journal of Rock Mechanics and Geotechnical Engineering, 6(2), 138–149. https://doi.org/10.1016/j.jrmge.2014.01.007

Refsgaard, J. C., Auken, E., Bamberg, C. A., Christensen, B. S. B., Clausen, T., Dalgaard, E., Effersø, F., Ernsten, V., Gertz, F., Hansen, A. L., He, X., Jacobsen, B. H., Jensen, K. H., Jørgensen, F., Jørgensen, L., F., Koch, J., Nilsson, B., Peterson, C., De Schepper, G., Schamper, C., Sørensen, K. I., Therrien, R., Thirup, C. & Viezzoli, A. (2014). Science of the Total Environment Nitrate reduction in geologically heterogeneous catchments - A framework for assessing the scale of predictive capability of hydrological models. Science of the Total Environment. 468–469, 1278–1288. https://doi.org/10.1016/j.scitotenv.2013.07.042

1398 Revil, A. (2005). Self-potential signals associated with preferential ground water flow pathways in a
1399 buried paleo-channel. Geophysical Research Letters, 32(7), L07401, 1–4.
1400 https://doi.org/10.1029/2004GL022124

1401 Revil, A., Mendonc, C. A., Atekwana, E. A., Kulessa, B., & Hubbard, S. S. (2010). Understanding
1402 biogeobatteries: Where geophysics meets microbiology. Journal of Geophysical Research,
1403 115, G00G02, 1–22. https://doi.org/10.1029/2009JG001065

1404 Revil, A. (2012). Spectral induced polarization of shaly sands: Influence of the electrical double layer.
1405 Water Resources Research, 48(2), 1–23. https://doi.org/10.1029/2011WR011260

1406 Richards, L. A., Magnone, D., van Dongen, B. E., & Polya, D. A. (2017). High Resolution Profile of
1407 Inorganic Aqueous Geochemistry and Key Redox Zones in an Arsenic Bearing Aquifer in
1408 Cambodia. Science of the Total Environment, 590–591, 540–553.
1409 https://doi.org/10.1016/j.scitotenv.2017.02.217

1410 Rizzo, E., Suski, B., & Revil, A. (2004). Self-potential signals associated with pumping tests experiments.
1411 Journal of Geophysical Research: Solid Earth, 109, B10203, 1–14.
1412 https://doi.org/10.1029/2004JB003049

1413 Robinson, D. A., Abdu, H., Lebron, I., & Jones, S. B. (2012). Imaging of hill-slope soil moisture wetting
1414 patterns in a semi-arid oak savanna catchment using time-lapse electromagnetic induction.
1415 Journal of Hydrology, 416–417, 39–49. https://doi.org/10.1016/j.jhydrol.2011.11.034

1416 Robinson, D. A., Lebron, I., Kocar, B., Phan, K., Sampson, M., & Crook, N. (2009). Time-lapse
1417 geophysical imaging of soil moisture dynamics in tropical deltaic soils: An aid to interpreting
1418 hydrological and geochemical processes, 45, 1–12. https://doi.org/10.1029/2008WR006984

1419 Rosenberry, D. O., & LaBaugh, J. W. (2008). Field techniques for estimating water fluxes between
1420 surface water and ground water techniques and methods. US Geological Survey Techniques
1421 and Methods 4–D2, 1–128. http://pubs.usgs.gov/tm/04d02/

1422 Rubin, Y., Hubbard, S. S. (Editors) (2005). Hydrogeophysics. Netherlands: Springer.

1423 Sassen, D. S., Hubbard, S. S., Bea, S. A., Chen, J., Spycher, N., & Denham, M. E. (2012). Reactive facies:
1424 An approach for parameterizing field-scale reactive transport models using geophysical
1425 methods. Water Resources Research, 48(10), W10526, 1–20.
1426 https://doi.org/10.1029/2011WR011047

1427 Sato, M., & Mooney, H. M. (1960). The electrochemical mechanism of sulfide self-potentials.
1428 Geophysics, 25(1), 226-249. https://doi.org/10.1190/1.1438689

1429 Schmadel, N. M., Ward, A. S., Lowry, C. S., & Malzone, J. M. (2016). Hyporheic exchange controlled by
1430 dynamic hydrologic boundary conditions. Geophysical Research Letters, 43, 4408–4417.
1431 https://doi.org/10.1002/2016GL068286

1432 Schmitt, D. R. (2015). Geophysical properties of the Near Surface Earth: Seismic Properties. In:
1433 Schubert, G. (Editor). Treatise on Geophysics, 2nd Edition, Vol. 11. Oxford, UK: Elsevier. P43-
1434 87.

1435 Shanahan, P. W., Binley, A., Whalley, W. R., & Watts, C. W., (2015). The Use of Electromagnetic
1436 Induction to Monitor Changes in Soil Moisture Profiles beneath Different Wheat Genotypes.
1437 Soil Science Society of America Journal, 79, 459-466.

1438 Singha, K., Day-Lewis, F. D., & Moysey, S. (2007). Accounting for Tomographic Resolution in Estimating
1439 Hydrologic Properties from Geophysical Data. In: Hyndman, D. W., Day-Lewis, F. D. & Singha,
1440 K. Subsurface Hydrology: Data Integration for Properties and Processes. AGU Geophysical
1441 Monograph Series, Vol. 171, p227–241. https://doi.org/10.1029/171GM16

1442 Singha, K., Pidlisecky, A., Day-Lewis, F. D., & Gooseff, M. N. (2008). Electrical characterization of non-
1443 Fickian transport in groundwater and hyporheic systems. Water Resources Research, 44(4),
1444 W00D07, 1–14. https://doi.org/10.1029/2008WR007048

1445 Singha, K., Day-Lewis, F. D., Johnson, T., & Slater, L. D. (2015). Advances in interpretation of subsurface
1446 processes with time-lapse electrical imaging. Hydrological Processes, 29(6), 1549–1576.
1447 https://doi.org/10.1002/hyp.10280

1448 Slater, L. D., Binley, A., & Brown, D. (1997). Electrical Imaging of Fractures Using Ground-Water Salinity
1449 Change. Ground Water, 35(3), 436–442. https://doi.org/10.1111/j.1745-
1450 6584.1997.tb00103.x

1451 Slater, L., & Lesmes, D. P. (2002). Electrical-hydraulic relationships observed for unconsolidated
1452 sediments. Water Resources Research, 38(10), 33–46.
1453 https://doi.org/10.1029/2001WR001075

1454 Slater, L., & Binley, A. (2006). Synthetic and field-based electrical imaging of a zerovalent iron barrier:
1455 Implications for monitoring long-term barrier performance. Geophysics, 71(5), B129–B137.
1456 https://doi.org/10.1190/1.2235931

1457 Slater, L. (2007). Near surface electrical characterization of hydraulic conductivity: From petrophysical
1458 properties to aquifer geometries - A review. Surveys in Geophysics, 28(2), 169–197.
1459 https://doi.org/10.1007/s10712-007-9022-y

1460 Slater, L., Ntarlagiannis, D., Yee, N., O'Brien, M., Zhang, C., & Williams, K. H. (2008). Electrodic voltages
1461 in the presence of dissolved sulfide: Implications for monitoring natural microbial activity.
1462 Geophysics, 73(2), F65–F70. http://doi.org/10.1190/1.2828977

1463 Slater, L. D., Ntarlagiannis, D., Day-Lewis, F. D., Mwakanyamale, K., Versteeg, R. J., Ward, A.,
1464 Strickland, C., Johnson, C. D., & Lane, J. W. (2010). Use of electrical imaging and distributed

temperature sensing methods to characterize surface water-groundwater exchange regulating uranium transport at the Hanford 300 Area, Washington. Water Resources Research, 46(10), W10533, 5–13. https://doi.org/10.1029/2010WR009110

Snyder, D.D. & Wightman, W.E. (2002). Application of continuous resistivity profiling to aquifer characterization. Proceedings of the 15th Symposium on the Application of Geophysics to Engineering and Environmental Problems, Las Vegas, Nevada, USA, Paper 13GSL10.

Sophocleous, M. (2002). Interactions between groundwater and surface water: the state of the science. Hydrogeology Journal, 10(1), 52–67. https://doi.org/10.1007/s10040-001-0170-8

Soueid Ahmed A., Jardani, A., Revil, A., & J.P. Dupont. (2014). Hydraulic conductivity field characterization from the joint inversion of hydraulic heads and self-potential data. Water Resources Research, **50**, 3502–3522.

Soueid Ahmed A., Jardani, A., Revil, A., & J.P. Dupont. (2016). Joint inversion of hydraulic head and self-potential data associated with harmonic pumping tests. Water Resources Research, 52(9), 6769–6791.

Stanford, J. A., & Ward, J. V. (1988). The hyporheic habitat of river ecosystems. Nature, 335(6185), 64–66. https://doi.org/10.1038/335064a0

Stanford, J. A., & Ward, J. V. (1993). An Ecosystem Perspective of Alluvial Rivers: Connectivity and the Hyporheic Corridor. Journal of the North American Benthological Society, 12(1), 48–60. https://doi.org/10.2307/1467685

Steeples, D. W. (2005). Shallow Seismic Methods. In: Rubin, Y. & Hubbard, S. S. (Editors). Hydrogeophysics, Vol. 2. Netherlands: Springer. p215–251.

1486 Stoll, J. B. (2013). Unmanned aircraft systems for rapid near surface geophysical measurements.
1487 International Archives of the Photogrammetry, Remote Sensing and Spatial Information
1488 Sciences, XL-1/W2, 391–394.

1489 Stonedahl, S. H., Harvey, J. W., Wörman, A., Salehin, M., & Packman, A. I. (2010). A multiscale model
1490 for integrating hyporheic exchange from ripples to meanders. Water Resources Research,
1491 46(12), W12539, 1–14. https://doi.org/10.1029/2009WR008865

1492 Stonedahl, S. H., Harvey, J. W., & Packman, A. I. (2013). Interactions between hyporheic flow produced
1493 by stream meanders, bars, and dunes. Water Resources Research, 49(9), 5450–5461.
1494 https://doi.org/10.1002/wrcr.20400

1495 Stonestrom, D. A., & Constantz, J. (2003). Heat as a tool for studying the movement of ground water
1496 near streams. US Geological Survey Circular 1260. p1–96. https://doi.org/SBN 0-607-94071-
1497 9

1498 Swarzenski, P. W., Simonds, F. W., Paulson, T., & Kruse, S. (2007) Geochemical and geophysical
1499 examination of submarine groundwater discharge and associated nutrient loading estimates
1500 into Lynch Cove, Hood Canal, WA. US Geological Survey Environmental Science and
1501 Technology, 41(20), 7022–7029. http://pubs.er.usgs.gov/publication/70031439

1502 Tarantola, A. (2005). Inverse problem theory and methods for model parameter estimation.
1503 Philadelphia, US: Society for Industrial and Applied Mathematics
1504 https://doi.org/10.1137/1.9780898717921

1505 Telford, W. M., Geldart, R. E. & Sheriff, R. E. (2010) Applied Geophysics, 2nd Edition. Cambridge, UK:
1506 Cambridge University Press.

1507 Tonina, D., & Buffington, J. M. (2007). Hyporheic exchange in gravel bed rivers with pool-riffle
1508 morphology : Laboratory experiments and three-dimensional modeling. Water Resources
1509 Research, 43, 1–16. https://doi.org/10.1029/2005WR004328

1510 Tonina, D., & Buffington, J. M. (2009). Hyporheic Exchange in Mountain Rivers I: Mechanics and
1511 Environmental Effects. Geography Compass, 3(3), 1063–1086.

1512 Topp, G. C., Davis, J. L., & Annan, A. P. (1980). Electromagnetic Determination of Soil Water Content:
1513 Water Resources Research, 16(3), 574–582. https://doi.org/10.1029/WR016i003p00574

1514 Toran, L., Hughes, B., Nyquist, J., & Ryan, R. (2012). Using hydrogeophysics to monitor change in
1515 hyporheic flow around stream restoration structures. Environmental and Engineering
1516 Geoscience, 18(1), 83–97. https://doi.org/10.2113/gseegeosci.18.1.83

1517 Toran, L., Hughes, B., Nyquist, J., & Ryan, R. (2013b). Freeze core sampling to validate time-lapse
1518 resistivity monitoring of the hyporheic zone. Ground Water, 51(4), 635–40.
1519 https://doi.org/10.1111/j.1745-6584.2012.01002.x

1520 Toran, L., Nyquist, J. E., Fang, A. C., Ryan, R. J., & Rosenberry, D. O. (2013a). Observing lingering
1521 hyporheic storage using electrical resistivity: Variations around stream restoration
1522 structures, Crabby Creek, PA. Hydrological Processes, 27(10), 1411–1425.
1523 https://doi.org/10.1002/hyp.9269

1524 Tóth, J. (1963). A Theoretical Analysis of Groundwater Flow in Small Drainage Basins. Journal of
1525 Geophysical Research, 68(16), 4795–4812.

1526 Triska, F. J., Kennedy, V. C., Avanzino, R. J., Zellweger, G. W., & Bencala, K. E. (1989). Retention and
1527 Transport of Nutrients in a Third-Order Stream in Northwestern California: Hyporheic
1528 Processes. Ecology, 70(6), 1893–1905. http://www.jstor.org/stable/1938120

1529

1530 Triska, F. J., Duff, J. H., & Avanzino, R. J. (1993). The role of water exchange between a stream channel
1531 and its hyporheic zone in nitrogen cycling at the terrestrial aquatic interface. Hydrobiologia,
1532 251(1–3), 167–184. https://doi.org/10.1007/BF00007177

1533 Tso, C.-H. M., Kuras, O., Wilkinson, P., Uhlemann, S., Chambers, J., Meldrum, P., Graham, J., Sherlock,
1534 E., & Binley, A. (in review). Improved characterisation and modelling of measurement errors
1535 in electrical resistivity tomography (ERT) surveys. Journal of Applied Geophysics.

1536 Uhlemann, S. S., Sorensen, J. P. R., House, A. R., Wilkinson, P. B., Roberts, C., Gooddy, D. C., Binley, A.
1537 M., & Chambers, J. E. (2016). Integrated time-lapse geoelectrical imaging of wetland
1538 hydrological processes. Water Resources Research, 52(3), 1607–1625.
1539 https://doi.org/10.1002/2015WR017932

1540 Uhlemann, S., O. Kuras, L. A. Richards, E. Naden, and D. A. Polya (2017), Electrical Resistivity
1541 Tomography determines the spatial distribution of clay layer thickness and aquifer
1542 vulnerability, Kandal Province, Cambodia, Journal of Asian Earth Sciences. Advance online
1543 publication. https://doi.org/10.1016/j.jseaes.2017.07.043

1544 Valett, H. M., Hakenkamp, C. C., & Boulton, A. J. (1993). Perspectives on the Hyporheic Zone:
1545 Integrating Hydrology and Biology. Journal of the North American Benthological Society.
1546 12(1), 40-43. http://www.jstor.org/stable/1467683 12

1547 van der Kruk, J. (2015). Tools and Techniques: Ground-Penetrating Radar. In: Schubert, G. (Editor).
1548 Treatise on Geophysics, 2nd Edition, Vol. 11. Oxford, UK: Elsevier. p209–232
1549 https://doi.org/10.1016/B978-0-444-53802-4.00195-0

1550 Viezzoli, A., Tosi, L., Teatini, P., & Silvestri, S. (2010). Surface water-groundwater exchange in
1551 transitional coastal environments by airborne electromagnetics: The Venice Lagoon
1552 example. Geophysical Research Letters, 37(1), L01402, 1–6.
1553 https://doi.org/10.1029/2009GL041572

1554 Vinegar, H. J. & Waxman, M. H. (1984). Induced polarization of shaly sands. Geophysics, 49(8), 1267-
1555 1287. https://doi.org/10.1190/1.1441755

1556 von Gunten, H. R., & Lienert, C. (1993). Decreased metal concentrations in ground water caused by
1557 controls of phosphate emissions. Nature, 364, 220–222.

1558 Voytek, E. B., Rushlow, C. R., Godsey, S. E., Singha, K., Science, H., Program, E., & Engineering, G.
1559 (2016). Identifying hydrologic flowpaths on arctic hillslopes using electrical resistivity and self
1560 potential. Geophysics, 81(1), 1–31. https://doi.org/10.1190/GEO2015-0172.1

1561 Wallin, E. L., Johnson, T. C., Greenwood, W. J., & Zachara, J. M. (2013). Imaging high stage river-water
1562 intrusion into a contaminated aquifer along a major river corridor using 2-D time-lapse
1563 surface electrical resistivity tomography. Water Resources Research, 49(3), 1693–1708.
1564 https://doi.org/10.1002/wrcr.20119

1565 Ward, A. S., Singha, K., & Gooseff, M. N. (2010a). Imaging hyporheic zone solute transport using
1566 electrical resistivity. Hydrological Processes, 24(7), 948–953.
1567 https://doi.org/10.1002/hyp.7672

1568 Ward, A. S., Gooseff, M. N., & Singha, K. (2010b). Characterizing hyporheic transport processes -
1569 Interpretation of electrical geophysical data in coupled stream-hyporheic zone systems
1570 during solute tracer studies. Advances in Water Resources, 33(11), 1320–1330.
1571 https://doi.org/10.1016/j.advwatres.2010.05.008

1572 Ward, A. S., Gooseff, M. N., & Singha, K. (2013). How does subsurface characterization affect
1573 simulations of hyporheic exchange? Ground Water, 51(1), 14–28.
1574 https://doi.org/10.1111/j.1745-6584.2012.00911.x

1575 Ward, A. S. (2016). The evolution and state of interdisciplinary hyporheic research. Wiley
1576 Interdisciplinary Reviews: Water, 383–103. https://doi.org/10.1002/wat2.1120

1577 Waxman, M. H., & Smits, L. J. M. (1968). Electrical Conductivities in Oil-Bearing Shaly Sands. Society of
1578 Petroleum Engineers Transactions, 243, 107–122. https://doi.org/10.2118/1863-A

1579 Webb, D. J., Anderson, N. L., Newton, T., & Cardimona, S. (2000). Bridge Scour: Application of Ground
1580 Penetrating Radar. Federal Highway Administration and Missouri Department of
1581 Transportation Special Publication, 1–19.

1582 Webster, I. T., Norquay, S. J., Ross, F. C., & Wooding, R. A. (1996). Solute Exchange by Convection
1583 within Estuarine Sediments. Estuarine, Coastal and Shelf Science, 42(2), 171–183.
1584 https://doi.org/10.1006/ecss.1996.0013

1585 Weller, A., Slater, L., & Nordsiek, S. (2013). On the relationship between induced polarization and
1586 surface conductivity: Implications for petrophysical interpretation of electrical
1587 measurements. Geophysics, 78(5), D315–D325. https://doi.org/10.1190/geo2013-0076.1

1588 Weller, A., Slater, L., Binley, A., Nordsiek, S., & Xu, S. (2015a). Permeability prediction based on
1589 induced polarization: Insights from measurements on sandstone and unconsolidated
1590 samples spanning a wide permeability range. Geophysics, 80(2), D161–D173.
1591 https://doi.org/10.1190/geo2014-0368.1

1592 Weller, A., Slater, L., Huisman, J. A., Esser, O., & Haegel, F. (2015b). On the specific polarizability of
1593 sands and sand-clay mixtures. Geophysics, 80(3), A57–A61.
1594 https://doi.org/10.1190/GEO2014-0509.1

1595 Weller, A., & Slater, L. D. (2015c). Induced polarization dependence on pore space geometry:
1596 Empirical observations and mechanistic predictions. Journal of Applied Geophysics, 123,
1597 310–315. https://doi.org/10.1016/j.jappgeo.2015.09.002

1598 Whitehead, K., Hudenholtz, C. H. (2014a). Remote Sensing of the Environment with Small Unmanned
1599 Aircraft Systems (UASs) Part 1: A review of progress and challenges. Journal of Unmanned
1600 Vehicle Systems, 2014, 2(3), 69–85.

1601 Whitehead, K., Hugenholtz, C. H., Myshak, S., Brown, O., LeClair, A., Tamminga, A., Barchyn, T. E.,
1602 Moorman, B., & Eaton, B. (2014b). Remote sensing of the environment with small
1603 unmanned aircraft systems (UASs) Part 2: Scientific and commercial applications. Journal of
1604 Unmanned Vehicle Systems, 2014, 2(3), 86–102.

1605 Wilkinson, P.B., Meldrum, P.I., Chambers, J.E., Kuras, O., & Ogilvy, R. (2006) Improved strategies for
1606 the automatic selection of optimized sets of electrical resistivity tomography measurement
1607 configurations. Geophysical Journal International, 167(3), 1119–1126.

1608 Wilkinson, P. B., Meldrum, P. I., Kuras, O., Chambers, J. E., Holyoake, S. J., & Ogilvy, R. D. (2010). High-
1609 resolution Electrical Resistivity Tomography monitoring of a tracer test in a confined aquifer.
1610 Journal of Applied Geophysics, 70(4), 268–276.
1611 https://doi.org/10.1016/j.jappgeo.2009.08.001

1612 Wilkinson, P. B., Loke, M. H., Meldrum, P. I., Chambers, J. E., Kuras, O., Gunn, D. A., & Ogilvy, R. D.
1613 (2012). Practical aspects of applied optimised survey design for electrical resistivity
1614 tomography. https://doi.org/10.1111/j.1365-246X.2012.05372.x/pdf

1615 Williams, B.A., Thompson, M.D., & Miller, S.F. (2012a). Integrated Surface Geophysical Investigation
1616 Results at Liquid Effluent Retention Facility, 200 East Area, Hanford, Washington. CH2MHill
1617 Plateau Remediation Company.

1618 Williams, B.A., Thompson, M.D., & Miller, S.F. (2012b).Interpretation and Integration of Seismic Data
1619 in the Gable Gap. CH2MHill Plateau Remediation Company.

Williams, B.A., Thompson, M.D., & Miller, S.F. (2012c). Land streamer and Gimbaled Geophones Phase II-200 Areas: High-Resolution Seismic Reflection Survey at the Hanford Site. CH2MHill Plateau Remediation Company.

Williams, B.A., Thompson, M.D., & Miller, S.F. (2012d). Seismic Reflection Investigation at the Liquid Effluent Retention Facility, 200 East Area, Hanford Site Richland, Washington. CH2MHill Plateau Remediation Company.

Williams, K. H., Ntarlagiannis, D., Slater, L. D., Dohnalkova, A., Hubbard, S. S., & Banfield, J. F. (2005). Geophysical imaging of stimulated microbial biomineralization. Environmental Science & Technology, 39(19), 7592–7600. http://doi.org/10.1021/es0504035

Wilson, J., Coxon, C., & Rocha, C. (2016). A GIS and remote sensing based screening tool for assessing the potential for groundwater discharge to lakes in Ireland. Biology and Environment: Proceedings of the Royal Irish Academy, 116B(3), 265–277. https://doi.org/10.3318/bioe.2016.15

Winter, T. (1976). Numerical Simulation Analysis of the Interaction of Lakes and Groundwater. US Geological Survey Professional Paper 1001, 1–45. https://pubs.er.usgs.gov/publication/pp1001

Winter, T. C., Harvey, J. W., Franke, O. L., & Alley, W. M. (1998). Ground water and surface water: A single resource. US Geological Survey Circular 1139, 1–79.

Wishart, D. N., Slater, L. D., & Gates, A. E. (2006). Self potential improves characterization of hydraulically-active fractures from azimuthal geoelectrical measurements. Geophysical Research Letters, 33(17), 2–6. https://doi.org/10.1029/2006GL027092

1641 Wishart, D. N., Slater, L. D., & Gates, A. E. (2008). Fracture anisotropy characterization in crystalline
1642 bedrock using field-scale azimuthal self potential gradient. Journal of Hydrology, 358(1–2),
1643 35–45. https://doi.org/10.1016/j.jhydrol.2008.05.017

1644 Woessner, W. W. (2000). Stream and Fluvial Plain Ground Water Interactions: Rescaling
1645 Hydrogeological Thought. Ground Water, 38(3), 423–429.

1646 Wojnar, A. J., Mutiti, S., & Levy, J. (2013). Assessment of geophysical surveys as a tool to estimate
1647 riverbed hydraulic conductivity. Journal of Hydrology, 482, 40–56.
1648 https://doi.org/10.1016/j.jhydrol.2012.12.018

1649 Wondzell, S. M., Gooseff, M. N., & McGlynn, B. L. (2010). An analysis of alternative conceptual models
1650 relating hyporheic exchange flow to diel fluctuations in discharge during baseflow recession.
1651 Hydrological Processes, 24(6), 686–694. https://doi.org/10.1002/hyp.7507

1652 Worrall, L., Munday, T. J., & Green, A. A. (1999). Airborne electromagnetics - Providing new
1653 perspectives on geomorphic process and landscape development in regolith-dominated
1654 terrains. Physics and Chemistry of the Earth, 24(10), 855–860.
1655 https://doi.org/10.1016/S1464-1895(99)00127-1

1656 Wynn, J. C., & Sherwood, S. I. (1984). The Self-Potential (SP) Method: An Inexpensive Reconnaissance
1657 and Archaeological Mapping Tool. Journal of Field Archaeology, 11(2), 195–204.
1658 https://doi.org/10.1179/jfa.1984.11.2.195

1659 Xie, Y., Cook, P. G., Shanafield, M., Simmons, C. T., & Zheng, C. (2016). Uncertainty of natural tracer
1660 methods for quantifying river-aquifer interaction in a large river. Journal of Hydrology, 535,
1661 135–147. https://doi.org/10.1016/j.jhydrol.2016.01.071

1662 Yoshikawa, K., & Hinzman, L. D. (2003). Shrinking thermokarst ponds and groundwater dynamics in
1663 discontinuous permafrost near Council, Alaska. Permafrost and Periglacial Processes, 14(2),
1664 151–160. https://doi.org/10.1002/ppp.451

1665 Zarroca, M., Linares, R., Rodellas, V., Garcia-Orellana, J., Roqué, C., Bach, J., & Masqué, P. (2014).
1666 Delineating coastal groundwater discharge processes in a wetland area by means of
1667 electrical resistivity imaging, 224Ra and 222Rn. Hydrological Processes, 28(4), 2382–2395.
1668 https://doi.org/10.1002/hyp.9793

1669 Zhang, J., & Revil, A. (2015). 2D joint inversion of geophysical data using petrophysical clustering and
1670 facies deformation. Geophysics, 80(5), M69–M88. https://doi.org/10.1190/geo2015-0147.1

1671 Zhou, B., & Greenhalgh, S. A. (2000). Cross-hole resistivity tomography using different electrode
1672 configurations. Geophysical Prospecting, 48(5), 887–912. https://doi.org/10.1046/j.1365-
1673 2478.2000.00220.x

1674 Zhou, J., Revil, A., Karaoulis, M., Hale, D., Doetsch, J., & Cuttler, S. (2014). Image-guided inversion of
1675 electrical resistivity data. Geophysical Journal International, 197(1), 292–309.
1676 https://doi.org/10.1093/gji/ggu001

1677 Zimmer, M. A., & Lautz, L. K. (2014). Temporal and spatial response of hyporheic zone geochemistry to
1678 a storm event. Hydrological Processes, 28(4), 2324–2337. https://doi.org/10.1002/hyp.9778